Research Square

Preprints are preliminary reports that have not undergone peer review.
They should not be considered conclusive, used to inform clinical practice,
or referenced by the media as validated information.

Bioinformatics and Machine Learning Internal Validation Reveal the Mechanism by Which β-Ecdysterone Combined with Paeoniflorin Alleviates Oxidative Stress-Induced Damage in Parkinson's Disease via the Nrf2 Pathway

Xinmin Shi
Qiqihar Medical University
Jiaxiang Zhao
Qiqihar Medical University
Xiaoming Li
Qiqihar Medical University
Xu Li
Qiqihar Medical University
Haiying Dong
Qiqihar Medical University
Jingyan Zhang
Qiqihar Medical University
Tianjiao Xu
Qiqihar Medical University
Chunlei Yu[1]
Qiqihar Medical University
Hui Li[1]
Qiqihar Medical University
Rong Hua
ronghua@qmu.edu.cn
Qiqihar Medical University

Research Article

Keywords: β-ecdysone, paeoniflorin, Parkinson's disease, oxidative stress, bioinformatics, machine learning

Posted Date: November 12th, 2026

DOI: https://doi.org/10.21203/rs.3.rs-11520778/v1

License: This work is licensed under a Creative Commons Attribution 4.0 International License.
Read Full License

Additional Declarations: No competing interests reported.

Bioinformatics and Machine Learning Internal Validation Reveal the Mechanism by Which β-Ecdysterone Combined with Paeoniflorin Alleviates Oxidative Stress-Induced Damage in Parkinson's Disease via the Nrf2 Pathway

Xinmin Shi, Jiaxiang Zhao[1],Xiaoming Li[1], Xu Li[1], Haiying Dong[1], Jingyan Zhang[1], Tianjiao Xu[1], Chunlei Yu[1], Hui Li[1] , Rong Hua[1,2*]

[1]Qiqihar Medical University, Qiqihar City, Heilongjiang, China;

[2]Postdoctoral Research Station, Qiqihar Institute of Medical Sciences, Qiqihar, Heilongjiang, China;

Corresponding Author: Rong Hua, Email:ronghua@qmu.edu.cn

Author：

Xinmin Shi：13100999443@163.com（First author，Female）

Qiqihar Medical University, Qiqihar City, Heilongjiang, China;

Jiaxiang Zhao：13199031485@163.com（Co-first author，Male）

Qiqihar Medical University, Qiqihar City, Heilongjiang, China;

Xiaoming Li：liming992@163.com Male

Qiqihar Medical University, Qiqihar City, Heilongjiang, China;

Xu Li：lx940762297@163.com Male

Qiqihar Medical University, Qiqihar City, Heilongjiang, China;

Haiying Dong：354498599@qq.com Female

Qiqihar Medical University, Qiqihar City, Heilongjiang, China;

Jingyan Zhang：276995008@qq.com Female

Qiqihar Medical University, Qiqihar City, Heilongjiang, China;

Tianjiao Xu：xutianjiaoler@126.com Female

Qiqihar Medical University, Qiqihar City, Heilongjiang, China;

Chunlei Yu：yuchunlei529@qmu.edu.cn Male

Qiqihar Medical University, Qiqihar City, Heilongjiang, China;

Hui Li：15635454183@126.com Female

Qiqihar Medical University, Qiqihar City, Heilongjiang, China;

Rong Hua：ronghua@qmu.edu.cn （Corresponding author） Female

Qiqihar Medical University, Qiqihar City, Heilongjiang, China;

Postdoctoral Research Station, Qiqihar Institute of Medical Sciences, Qiqihar, Heilongjiang, China;

Bioinformatics and Machine Learning Internal Validation Reveal the Mechanism by Which β-Ecdysterone Combined with Paeoniflorin Alleviates Oxidative Stress-Induced Damage in Parkinson's Disease via the Nrf2 Pathway

Xinmin Shi, Jiaxiang Zhao[1],Xiaoming Li[1], Xu Li[1], Haiying Dong[1], Jingyan Zhang[1], Tianjiao Xu[1], Chunlei Yu[1], Hui Li[1] , Rong Hua[1,2*]

[1]Qiqihar Medical University, Qiqihar City, Heilongjiang, China;

[2]Postdoctoral Research Station, Qiqihar Institute of Medical Sciences, Qiqihar, Heilongjiang, China;

[*]Corresponding Author: Rong Hua, Email:ronghua@qmu.edu.cn

Abstract: Background: Oxidative stress induces dopaminergic apoptosis and accelerates Parkinson's disease (PD). The Nrf2 pathway mediates central antioxidant defense. β-ecdysone (β-Ecd) and paeoniflorin (PF) produce Nrf2-dependent neuroprotection alone, while their combined anti-PD mechanism remains unknown. This study used bioinformatics, machine learning, molecular docking, 100-ns MD simulations and MPTP-PD mice to explore their synergy and Nrf2-mediated neuroprotection.**Methods:** TCMSP screened herbal ingredients. Drug-PD targets and PD DEGs were retrieved from databases and GEO. Overlapping targets underwent GO/KEGG enrichment; core targets filtered by LASSO, Random Forest and SVM-RFE were validated by independent GEO data.Molecular docking and 100 ns MD simulations assessed ligand-receptor binding. PD mice were divided into control, model, selegiline, β-Ecd, PF and combination groups. Motor function, nigral neuronal morphology, antioxidant indices and the expression of DA markers, total HSP90AA1, total and phosphorylated PRKCB and STAT3 ， Nrf2 downstream HO-1/NQO1 and apoptosis-related proteins were detected. **Results:** Twenty-two drug-disease intersecting targets were obtained. Enrichment analysis highlighted oxidative stress closely associated with Nrf2 signaling. STAT3, HSP90AA1 and PRKCB were identified as core targets. Molecular simulations verified favorable binding affinity between the two compounds and the three proteins. In PD mice, combined β-Ecd and PF reversed molecular abnormalities, activated Nrf2-dependent HO-1/NQO1, restored antioxidant capacity and suppressed neuronal apoptosis. Its neuroprotective effect was superior to single-drug treatment and comparable to selegiline. **Conclusions:** β-Ecd combined with PF protects dopaminergic neurons by targeting HSP90AA1-PRKCB-STAT3 and indirectly activating Nrf2 antioxidant signaling in PD mice.

Keywords: β-ecdysone; paeoniflorin; Parkinson's disease; oxidative stress; bioinformatics; machine learning

1. Introduction

PD is a common neurodegenerative disorder characterized by the loss of DA neurons in the substantia nigra pars compacta. Global PD prevalence is projected to rise by 50% by 2030. Typical motor manifestations, including resting tremor, rigidity, bradykinesia and postural instability, severely impair the health and quality of life of older adults [1–3]. Conventional treatments such as levodopa replacement and surgical intervention merely relieve PD symptoms and cannot reverse progressive neuronal degeneration. Long-term levodopa administration often induces adverse effects, including dyskinesia and reduced drug efficacy [4-5]. Although the etiology of PD remains incompletely defined, accumulating evidence indicates that oxidative stress drives neuronal death, and the Nrf2 antioxidant pathway is critical to PD pathogenesis [6–8].Growing attention has focused on bioactive constituents from traditional Chinese medicine for PD therapy. Niuxi, the dried root of Achyranthes bidentata Blume (Amaranthaceae), tonifies the liver and kidneys and directs fire downward. Its phytochemicals comprise steroidal ketones, alkaloids, saponins, polysaccharides, flavonoids and organic acids. Its major bioactive compounds include β-Ecd, berberine, coptisine, wogonin and quercetin. As the core ingredient of Achyranthes bidentata, β-Ecd (molecular structure in Figure 1) possesses potent antioxidant activity, which underlies its pharmacological actions [9–11].Paeoniflorin (PF, molecular structure in Figure 2) is the principal bioactive component of white peony root. PF exerts diverse bioactivities: anti-inflammatory, antioxidative, immunomodulatory, pro-autophagic and anti-apoptotic effects. It has shown therapeutic potential in multiple neurological disorders such as PD, cerebral ischemia, hypoxia and Alzheimer's disease[12–14].Herein, we integrated bioinformatics, machine learning screening, molecular docking, molecular dynamics simulations and in vivo animal assays to explore the neuroprotective effects of combined β-Ecd and PF against MPTP-triggered DA neuronal injury in PD mice and uncover the underlying mechanisms. We further validated whether bioinformatically screened targets HSP90AA1, PRKCB and STAT3 modulate the Nrf2 antioxidant pathway to attenuate oxidative damage. This study provides experimental support for developing natural active candidates for PD treatment.

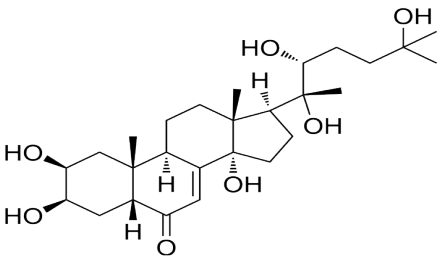


Figure 1. Molecular structure of β-Ecd.

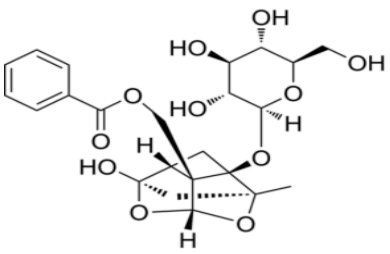


Figure 2. Molecular structure of PF.

2 Materials and Methods

2.1 Drugs and Reagents

β-Ecd (purity ≥98%, Cat. No. HY-N6979) and PF (purity ≥98%, Cat. No. HY-N0293) were purchased from MedChemExpress (MCE, USA). Sel hydrochloride tablets were purchased from Orion Corporation. MPTP was purchased from Sigma-Aldrich (St. Louis, MO, USA). Dopamine transporter (DAT, Cat. No. sc-32259) antibody was purchased from Santa Cruz Biotechnology, USA. Nrf2 antibody was purchased from Bioss, China. Heme oxygenase-1 (HO-1, Cat. No. AF1333) and NAD(P)H quinone dehydrogenase 1 (NQO-1, Cat. No. AF7614) antibodies were obtained from Beyotime, China. Tyrosine hydroxylase (TH, Cat. No. BM1609), heat shock protein 90 alpha family class A member 1 (HSP90AA1, Cat. No. PB0681), protein kinase C β (PRKCB, Cat. No. A01940), phosphorylated PRKCB (p-PRKCB, Cat. No. P01940), signal transducer and activator of transcription 3 (STAT3, Cat. No. PB0540), phosphorylated STAT3 (p-STAT3, Cat. No. BM4835), Bcl-2 (Cat. No. A00040-1), BAX (Cat. No. A00183), β-actin (Cat. No. BM3873), and glyceraldehyde-3-phosphate dehydrogenase (GAPDH, Cat. No. BM1623) antibodies were obtained from Boster, China. Catalase (CAT, Cat. No. BC0200), superoxide dismutase (SOD, Cat. No. BC0170), and total antioxidant capacity (T-AOC, Cat. No. BC1315) assay kits were purchased from Solarbio, China. β-Ecd was dissolved in a minimal volume of DMSO and diluted with sterile saline. PF was dissolved in distilled water. MPTP was dissolved in normal saline.

2.2 Acquisition and preprocessing of public datasets

PD expression datasets GSE22491 and GSE49036 were downloaded from the GEO database (https://www.ncbi.nlm.nih.gov/geo/), and all analyses were performed in R (v4.4.2). The raw data were subjected to $\log_2(x+1)$ transformation and quantile normalization. According to probe annotation information from the GPL platform files, probe IDs were mapped to corresponding gene symbols. The mean value of multiple probes corresponding to the same gene was calculated to construct the expression matrix. Batch-effect correction was conducted using the ComBat algorithm. Duplicate genes and low-quality entries with non-finite expression values were removed to generate the final expression matrix for subsequent differential analysis.

2.3 Screening of differentially expressed genes (DEGs)

The limma package was applied to construct a linear model, and the empirical Bayes method was employed to perform statistical tests for gene expression differences between the control group and the PD group. Up-regulated and down-regulated DEGs were screened under the thresholds of $|\log_2 FC|>0.26$ and $P<0.05$. Principal component analysis (PCA) was carried out to evaluate the transcriptomic distribution of samples before and after batch-effect correction and assess intra-group homogeneity and inter-group separation. The ggplot2 and pheatmap packages were adopted to generate heatmaps of normalized DEGs and volcano plots annotated with key genes, so as to intuitively reflect transcriptomic differences among groups.

2.4 Screening of active compounds of Achyranthes bidentata and Paeonia lactiflora based on the TCMSP database

The TCMSP database was used to screen potential active ingredients of Achyranthes bidentata and Paeonia lactiflora. Oral bioavailability ≥30% and drug-likeness ≥0.18 were defined as screening thresholds to obtain candidate active components. β-Ecd and PF were selected as research objects for subsequent target prediction analysis.

2.5 Prediction of potential targets of β-Ecd and PF and intersection analysis of disease targets

Drug targets of β-Ecd and PF were predicted using SEA, SwissTargetPrediction and TargetNet databases. PD-related disease targets were retrieved from GeneCards, OMIM and TTD databases. Targets obtained from each database were deduplicated and merged separately, followed by Venn intersection analysis with pre-obtained DEGs to screen potential common targets of β-Ecd and PF against PD.

2.6 Construction of protein-protein interaction (PPI) network and screening of key targets

The above intersecting targets were imported into the STRING database(v12.5) for PPI network construction. The organism was set to Homo sapiens with medium-confidence combined score (≥0.4). Discrete nodes without interactions were discarded. The PPI data were imported into Cytoscape v3.9.1 for network construction and visualization.

2.7 GO/KEGG Enrichment Analysis

To explore the biological functions and signaling pathways of potential targets through which β-Ecd and PF exert their effects for PD intervention, GO functional enrichment and KEGG pathway enrichment analyses were performed on the intersecting targets using the clusterProfiler package (v4.10.0). GO enrichment was conducted across three categories: biological process (BP), cellular component (CC), and molecular function (MF). KEGG analysis was applied to identify key signaling pathways. The threshold for significantly enriched terms was defined as Benjamini–Hochberg (BH)-adjusted $P < 0.05$. The top 20 KEGG pathways ranked by $-\log_{10}$(P-value) were selected for visualization. The GO enrichment results were displayed in a circular plot, and the KEGG enrichment results were

presented using a Sankey diagram combined with a bubble plot to further interpret the association between core targets and key pathways.

2.8 Construction of Machine-Learning Models and Screening of Core Targets

Three machine-learning algorithms, including LASSO, random forest and linear-kernel SVM-RFE, were used to screen feature genes based on the standardized expression matrix. Only internal cross-validation was performed for the feature-screening step, and the external dataset GSE7621 was used for independent validation of core targets in downstream analyses (Section 2.9). For the LASSO elastic net model, α was set to 0.9. Ten-fold cross-validation was performed to determine the optimal λ value, and the top 10 genes with non-zero coefficients were screened. For the random forest model, ntree was set to 2000. The top 10 high-contribution genes were screened based on the MeanDecreaseGini index. The SVM-RFE algorithm combined with 5-fold cross-validation was used to identify the top 10 key genes. Genes within the Venn intersection derived from the three algorithms were defined as core targets to reduce single-algorithm bias. Combined with PPI network topological analysis, HSP90AA1, PRKCB and STAT3 were further screened from these core targets as key targets for subsequent molecular docking, molecular dynamics simulation and in vivo experimental validation.

2.9 Validation of Core Targets Using an Independent Dataset and Diagnostic Performance Analysis

The independent human transcriptomic dataset GSE7621 was used for external validation of the six core targets screened by machine learning. The expression levels of core genes were extracted from the validation dataset. Independent-sample t-tests were performed to compare gene expression differences between healthy controls and PD patients. The expression characteristics of core genes in clinical PD samples were analyzed. ROC curves were constructed based on the binary classification of healthy and PD status. AUC values and corresponding 95% confidence intervals were calculated to evaluate the discriminatory ability of each core gene. An AUC value greater than 0.5 was defined as the criterion for discriminating PD from healthy status.Single-gene and multi-gene combined ROC curves were plotted to visually compare the diagnostic efficiency of the six core targets.

2.10 Molecular Docking Simulation

AutoDock Vina 1.1.2 was used for molecular docking of β-Ecd and PF with three core target proteins. AutoDockTools 1.5.7 was used for structural preprocessing of receptor proteins and small-molecule ligands. Water molecules and heteroatoms were removed. Hydrogen atoms were added, and Gasteiger charges were calculated for receptors. For β-Ecd and PF ligands, hydrogen atoms were added, charges were calculated, and rotatable bonds were defined. All structural files were converted to pdbqt format. Docking computations were then performed. The conformation with the lowest binding free energy was selected as the optimal binding model. A more negative binding free-energy value indicated stronger binding stability of the ligand-receptor complex. PyMOL 2.5.7 was used to visualize non-covalent interactions, including hydrogen bonds and hydrophobic contacts, between ligands and amino

acid residues.

2.11 Molecular Dynamics Simulation

To further explore the dynamic stability and intermolecular interactions between β-Ecd, PF and core target proteins, 100 ns all-atom molecular dynamics simulations of two protein-ligand complexes were performed using GROMACS 2023.2. Protein structures were parameterized with the Amber99sb-ildn force field. The GAFF force field was utilized for β-Ecd and PF ligands, and AM1-BCC charges were assigned using the Antechamber program. Each complex was placed in a cubic periodic box, with a minimum distance of 1.2 nm between the protein and box wall, and solvated using the TIP3P water model. Na^+ and Cl^- ions were added to achieve a physiological ionic strength of 0.15 M. System energy minimization was performed using the steepest descent method until the maximum force was reduced below 500 kJ/(mol·nm). Subsequently, 1 ns equilibrium simulations were conducted under NVT (300 K) and NPT (1 bar) ensembles. Bond lengths were constrained by the LINCS algorithm, and a 2 fs time step was adopted for the 100 ns formal molecular dynamics simulation. Simulation trajectories were analyzed using the built-in tools of GROMACS. The backbone root-mean-square deviation (RMSD), residue root-mean-square fluctuation (RMSF), hydrogen bond number, radius of gyration (Rg) and solvent-accessible surface area (SASA) were calculated. The MM/PBSA method was applied to calculate the binding free energy. A free-energy landscape (FEL) was constructed based on RMSD and Rg to evaluate the conformational stability and thermodynamic characteristics of the complexes.

2.12 Experimental Animals

Male SPF-grade C57BL/6 mice, aged 6–8 weeks with body weights of 20–26 g, were supplied by the Laboratory Animal Center of Qiqihar Medical University. Animals were kept at ambient temperature of (23 ± 2) °C under a 12-h light-dark cycle, and allowed free access to food and water. The experiments were started following a one-week period of acclimatization. The animal study protocol was reviewed and approved by the Animal Ethics Committee of Qiqihar Medical University (Ethics No.: QMU-AECC-2025-232).

2.13 Animal Grouping and Drug Treatment

Mice were randomly assigned to six experimental groups: control group, MPTP-induced model group (30 mg/kg)[15], sel group (10 mg/kg)[16], β-Ecd group (2 mg/kg), PF group (20 mg/kg), and β-Ecd combined with PF group (β-Ecd 2 mg/kg + PF 20 mg/kg)[17]. Sel, β-Ecd and PF were intragastrically administered once daily for 14 consecutive days. Mice in the control and model groups were given an equal volume of distilled water. Starting from day 10, mice in all groups except the control group received intraperitoneal injections of MPTP for 5 consecutive days. Behavioral tests were carried out after model establishment, and tissue sampling was performed upon completion of the tests.

2.14 Behavioral tests

2.14.1 Pole-climbing test

Behavioral assessment via the pole-climbing test commenced upon completion of drug treatment. A 2.5 cm-diameter

plastic ball was affixed to the apex of a 50 cm-long acrylic pole (1.5 cm in diameter), whose surface was wrapped in gauze to avoid animal slippage. Mice were positioned atop the plastic sphere, and the latency to descend from the ball to the pole bottom was documented. Scoring criteria: 0 point, latency to descend＜4.01 s; 1 point, 4.01–8.00 s; 2 points, 8.01–12.00 s; 3 points, latency to descend＞12.00 s.

2.14.2 Rotarod test

At the end of drug administration, the rotarod test was performed. A unified rotarod protocol was adopted throughout the experiment, and the rotational speed was dynamically adjusted according to the motor performance of mice to ensure that the latency to the first fall of normal mice was no less than 200 s within a 5-min testing period. The latency to the first fall was recorded during the test to assess motor balance, coordination and endurance of mice.

2.14.3 Open-field test

Mice were placed into the central zone of the open-field arena (50 cm × 50 cm). The open-field test analysis system recorded the total travel distance and immobility duration of mice over a 5-min test period. After each test, the open-field arena was wiped with disinfectant to remove odors.

2.15 Hematoxylin-eosin (HE) staining

HE staining was performed according to the manufacturer's instructions using a commercial staining kit.Paraffin-embedded sections underwent standard xylene de-paraffinization and rehydration in graded ethanol, prior to triple PBS rinses lasting 3 min each. Tissue sections were subjected to hematoxylin staining, bluing in ammonia water, and subsequent eosin counterstaining. Dehydration, tissue clearing and slide mounting were then performed. Neuronal morphological alterations in the mouse substantia nigra (SN) were visualized under light microscopy.

2.16 Nissl staining

Nissl staining was performed using a commercial kit. Paraffin-embedded sections underwent conventional deparaffinization and full rehydration. Sections were incubated with methyl violet staining solution for 10-20 min. Excess dye was rinsed off with distilled water, followed by brief treatment with differentiation solution until the desired color was obtained. Dehydration with absolute ethanol and xylene clearing were performed sequentially, and sections were mounted with neutral balsam mounting medium. Observations of the number and morphological features of Nissl-positive neurons were carried out under a light microscope.

2.17 Immunohistochemistry (IHC)

Detection was performed using the DAB method. Mid-brain tissues were immersed and fixed in 4 % paraformaldehyde for 72 h, followed by dehydration, wax impregnation and paraffin embedding. After sectioning, deparaffinization and rehydration, antigen retrieval was performed. Sections were incubated with TH antibody (1:1000) overnight at 4 ℃. After washing with PBS, secondary antibody（1：3000）was added and incubated at room temperature

for 10 min. After color development with DAB working solution, sections were counter-stained with hematoxylin, fully rinsed with tap water for bluing, and mounted with neutral balsam mounting medium. The expression of TH-positive neurons in the SN region of mouse mid-brain was observed under a microscope. After image acquisition, ImageJ software was used to measure the area of positive-stained regions in each group for quantitative analysis.

2.18 Measurement of Antioxidant-Related Parameters

Mouse brain tissue was rapidly isolated on ice. Pre-chilled extraction buffer was added at a ratio of tissue weight (g): kit-specified extraction volume (mL) = 1:10, and the mixture was thoroughly homogenized in an ice bath. For SOD and CAT assays, samples were centrifuged at 8,000 g and 4 ℃ for 10 min; for T-AOC assays, samples were centrifuged at 10,000 rpm and 4 ℃ for 10 min. The supernatants were collected separately and kept on ice for subsequent analysis. Biochemical methods were used to measure CAT and SOD activities, as well as total antioxidant capacity (T-AOC), in mouse brain tissue from each group. Subsequent procedures were strictly performed in accordance with the Solarbio kit instructions. A UV-visible spectrophotometer was used to measure the absorbance (OD value) of the reaction mixtures, and the antioxidant enzyme activities and total antioxidant capacity levels of each group were calculated based on the standard curve.

2.19 Western Blot Assay

Brain tissue was rapidly harvested on ice. PMSF and phosphatase inhibitors were added to RIPA lysis buffer immediately before use for brain tissue protein extraction. Samples were centrifuged at 12,000 rpm for 10 min at 4 ℃. Protein concentrations were determined by the microplate method: absorbance was measured at 562 nm using a microplate reader, a standard curve was plotted, and sample protein concentrations were calculated. Following SDS-PAGE separation, proteins were transferred to PVDF membranes. Membranes were blocked overnight at 4 ℃, then incubated with the following primary antibodies: TH (1:1 000), DAT (1:400), HSP90AA1 (1:1000), PRKCB (1:1000), p-PRKCB (1:1000), STAT3 (1:3000), p-STAT3 (1:3000), Nrf2 (1:400), HO-1(1:1500), NQO-1(1:1000), Bcl-2(1:1000), BAX(1:1000), β-actin (1:2000), GAPDH (1:10000). Membranes were incubated with secondary antibodies at room temperature for 1.5 h. Membranes were washed three times with TBST, 10 min per wash. Protein bands were detected using an ECL kit and visualized with a Molecular Imager®245 ChemiDoc™ XRS+ imaging system. Band intensities were analyzed using ImageJ software. Quantification: Target protein expression was calculated as the band intensity ratio of target protein to the corresponding internal reference protein. Phosphorylation levels were defined as the ratio of phosphorylated protein band intensity to total protein band intensity, p-PRKCB/PRKCB and p-STAT3/STAT3. β-actin was used as the internal reference for PRKCB, STAT3, p-PRKCB, p-STAT3 and HSP90AA1; GAPDH served as the internal reference for the remaining proteins.

2.20 Statistical Analysis

All statistical analyses were performed using GraphPad Prism 10.1.2. Quantitative data are presented as mean ± standard deviation (X ± S), with sample sizes (n) indicated in figure and table legends. The Shapiro-Wilk test, Bartlett's test and Brown-Forsythe test were applied to evaluate normality and homogeneity of variances. Non-normal data were analyzed using the Kruskal-Wallis H test with adjusted Dunn's test and the Mann-Whitney U test. Normally distributed data with unequal variances were assessed by Welch's one-way ANOVA and Welch's t-test. For normally distributed data with homogeneous variances, an independent samples t-test was adopted for comparisons between the control and model groups. One-way ANOVA followed by Dunnett's multiple comparisons test was used to compare the model group with each treatment group. A P-value < 0.05 was considered statistically significant.

3. Results

3.1 Batch Correction and Identification of Differentially Expressed Genes in PD Transcriptomic Datasets

Two PD transcriptome datasets (GSE22491, GSE49036) were combined for integrated analysis. Pre-correction boxplots and PCA plots revealed prominent batch bias that distorted sample clustering. After normalization with the ComBat algorithm, sample expression profiles became homogeneous, and cross-dataset samples clustered closely in PCA, eliminating batch interference effectively (Figure 3a–d).Differentially expressed genes (DEGs) were screened via the limma package with thresholds $|\log_2 FC|>0.26$ and $P<0.05$. hierarchical clustering heatmaps displayed clear transcriptional divergence between control and PD groups, while volcano plots intuitively classified all genes into upregulated, downregulated and non-significant subsets (Figure 3e–f).

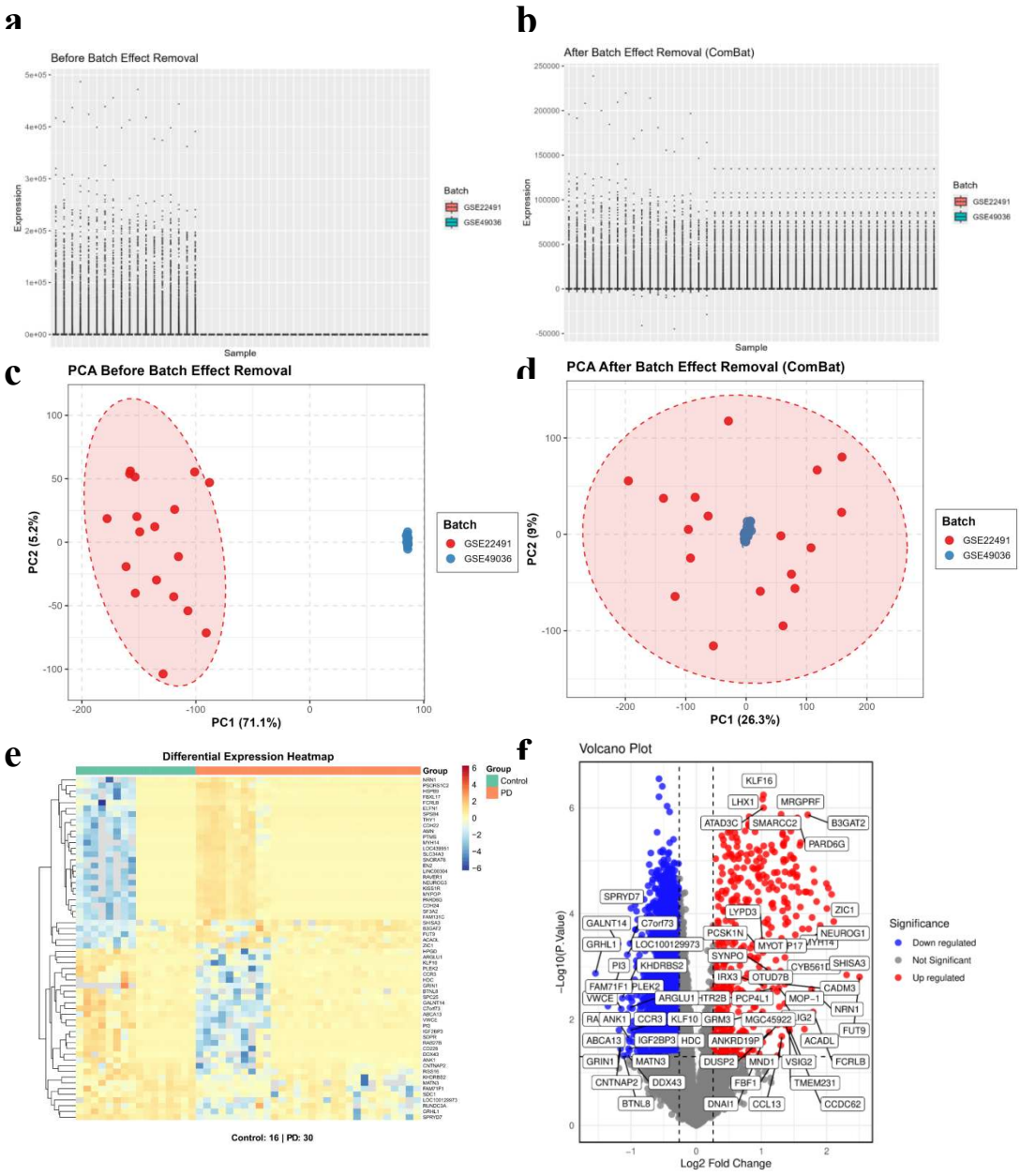


Figure 3. Batch correction of transcriptomic data and screening of differentially expressed genes (DEGs) in PD.

(a–b) Boxplots of gene expression before and after batch correction; (c–d) PCA plots before and after batch correction; (e) Heatmap of PD-related DEGs; (f) Volcano plot of PD-related DEGs.

3.2 Screening of Active Compounds from Achyranthes bidentata and Paeonia lactiflora

Chemical constituents of Achyranthes bidentata and Paeonia lactiflora were retrieved from the Traditional Chinese Medicine Systems Pharmacology Database (TCMSP). The database search yielded 194 constituents for Achyranthes bidentata and 53 constituents for Paeonia lactiflora. Active compounds were further filtered according to the thresholds

of oral bioavailability (OB) ≥ 30% and drug-likeness (DL) ≥ 0.18. Following screening, 16 active constituents from Achyranthes bidentata and 13 active constituents from Paeonia lactiflora were retained for subsequent analysis (Table 1 and Table 2).

Table 1. Screening results for active ingredients in Achyranthes bidentata

Drug	Number	MOLNumber	Molecule name	OB(%)	DL
Achyranthes bidentata	1	MOL001006	Poriferasta-7,22E-dien-3 beta-ol	42.98%	0.76
	2	MOL012461	28-norolean-17-en-3-ol	35.93%	0.78
	3	MOL012542	*β*-ecdysterone	44.23%	0.82
	4	MOL001454	Berberine	36.86%	0.78
	5	MOL001458	Coptisine	30.67%	0.86
	6	MOL000173	Wogonin	30.68%	0.23
	7	MOL002643	delta 7-stigmastenol	37.42%	0.75
	8	MOL002714	Baicalein	33.52%	0.21
	9	MOL002897	Epiberberine	43.09%	0.78
	10	MOL000358	beta-sitosterol	36.91%	0.75
	11	MOL000422	Kaempferol	41.88%	0.24
	12	MOL004355	Spinasterol	42.98%	0.76
	13	MOL000449	Stigmasterol	43.83%	0.76
	14	MOL000785	Palmatine	64.6%	0.65
	15	MOL000085	beta-daucosterol_qt	36.91%	0.75
	16	MOL000098	Quercetin	46.43%	0.28

Note: MOL Number: molecular ID ; OB: Oral bioavailability; DL: Drug-likeness.

Table 2.Screening results for active components in Paeonia lactiflora

Drug	Number	MOLNumber	Molecule name	OB(%)	D L
Paeonia lactiflora	1	MOL001910	11alpha,12alpha-epoxy-3beta-23-dihydroxy-30-norolean-20-en-28,12beta-olide	64.77	0.38
	2	MOL001918	Paeoniflorgenone	87.59	0.37
	3	MOL001919	(3S,5R,8R,9R,10S,14S)-3,17-dihydroxy-4,4,8,10,14-pentamethyl-2,3,5,6,7,9-hexahydro-1H-cyclopenta[a]phenanthrene-15,	43.56	0.53

		16-dione		
4	MOL001921	Lactiflorin	49.12	0.80
5	MOL001924	Paeoniflorin	53.87	0.79
6	MOL001925	Paeoniflorin_qt	68.18	0.40
7	MOL001928	Albiflorin_qt	66.64	0.33
8	MOL001930	Benzoyl paeoniflorin	31.27	0.75
9	MOL000211	Mairin	55.38	0.78
10	MOL000358	Beta-sitosterol	36.91	0.75
11	MOL000359	Sitosterol	36.91	0.75
12	MOL000422	Kaempferol	41.88	0.24
13	MOL000492	(+)-catechin	54.83	0.24

Note: MOL Number: molecular ID ; OB: Oral bioavailability; DL: Drug-likeness.

3.3 Screening and Bioinformatics Analysis of Overlapping Targets between Drugs and PD

3.3.1 Screening of Overlapping Drug Targets, Disease Targets and Differentially Expressed Genes

In the present study, 203 potential targets corresponding to combined β-Ecd and PF treatment, 5381 PD-associated targets, and 4008 PD differentially expressed genes (DEGs) were retrieved. The quantitative distribution of genes within the three datasets is illustrated in the bar graph (Figure 4a). Subsequent intersection analysis of the three gene sets yielded 22 shared targets, as visualized in the Venn diagram (Figure 4b).

3.3.2 Construction of the PPI Network of Overlapping Targets and Screening of Key Targets

The 22 overlapping targets derived from the intersection of drug targets, PD disease targets and PD differentially expressed genes were submitted to the STRING database for protein-protein interaction (PPI) analysis. The combined score threshold was set at ≥ 0.4, and three isolated nodes with no interactions were excluded. The resulting PPI network contained 19 nodes. Interaction data were imported into Cytoscape v3.9.1 for network visualization. Key targets with high connectivity were preliminarily screened based on the topological properties of the PPI network (Figure 4c).

3.3.3 GO and KEGG Functional Enrichment Analysis of Overlapping Targets

GO enrichment results (Figure 4d) indicated that overlapping targets were predominantly enriched in biological

processes (BP), including response to oxidative stress, reactive oxygen species metabolic process, modulation of neuronal apoptosis, and regulation of inflammatory responses. For cellular component (CC) terms, these targets were mainly distributed in the mitochondria, cell membrane and cytoplasm, the major compartments where oxidative stress occurs. Molecular function (MF) enrichment revealed prominent enrichment in transcription factor binding and protein kinase activity. KEGG pathway enrichment demonstrated that overlapping targets were significantly enriched in signaling pathways tightly associated with oxidative stress and neuroinflammation in PD pathology, such as the NF-κB, JAK-STAT, HIF-1 and PI3K-Akt signaling pathways (Figure 4e). These pathways represent upstream and downstream regulatory cascades that interact with the Nrf2 antioxidant pathway. Collectively, these findings implied that combined β-Ecd and PF treatment may indirectly modulate the Nrf2 pathway by regulating oxidative stress-related cascades, thereby alleviating oxidative stress injury in PD.

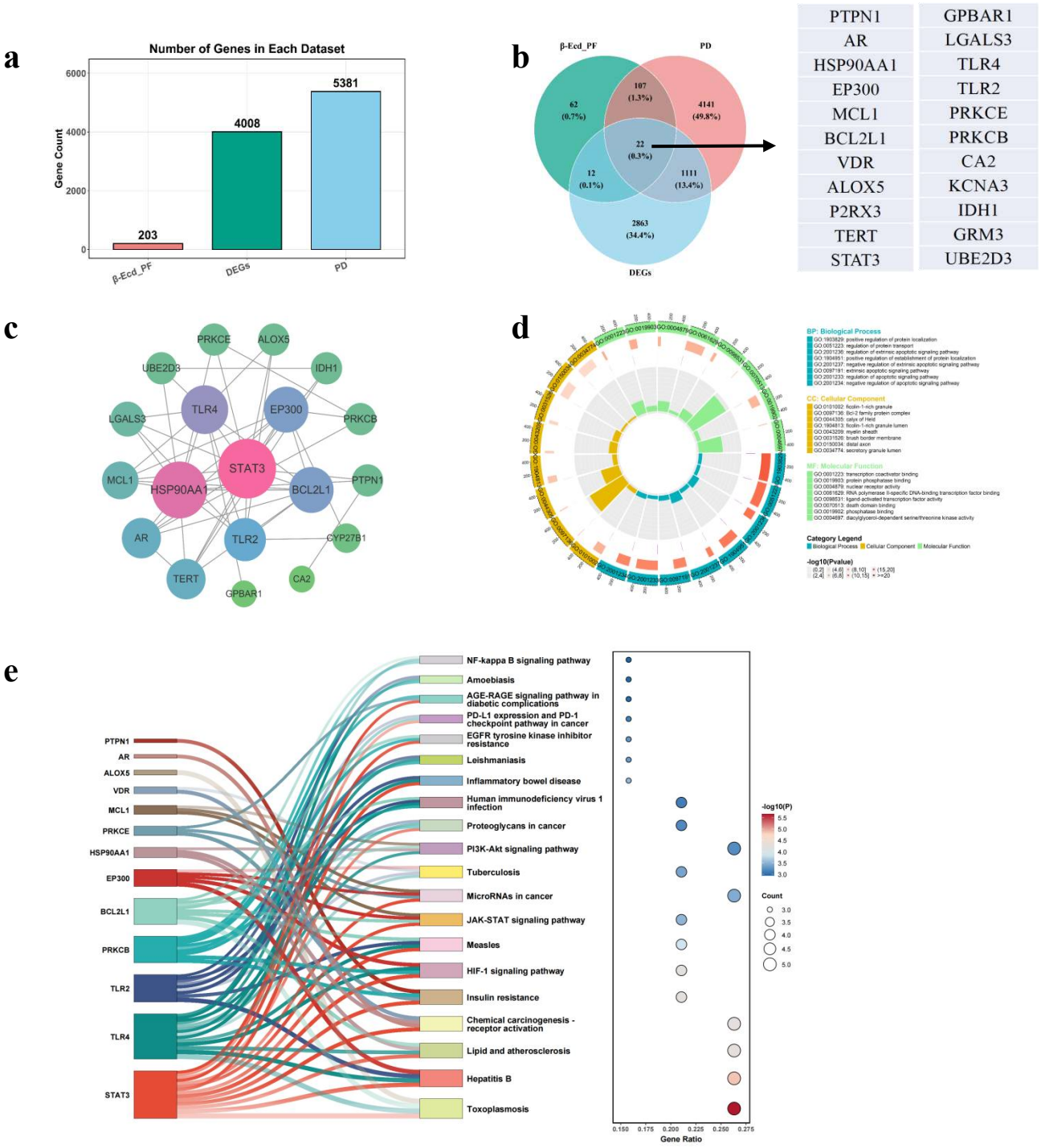


Figure 4. Core target screening, protein–protein interaction network, and functional enrichment analysis

(a) Bar plot showing gene counts for potential targets of β-Ecd combined with PF, PD DEGs, and PD disease targets; (b) Venn diagram displaying the intersection of the three gene sets, identifying 22 common potential targets; (c) Visualization of the PPI network; (d)Circular plot of GO functional enrichment;(e) Chord diagram of KEGG pathway enrichment.

3.4 Screening of Feature Genes via Machine Learning Algorithms

Three machine learning algorithms, namely SVM-RFE, random forest (RF), and LASSO regression, were applied to screen feature genes from the common drug–disease targets. For the SVM-RFE algorithm, the model attained the highest cross-validation accuracy and minimal error at a feature number of 2 (Figure. 5a–b), and the top 10 feature genes were identified accordingly (Figure. 5c). The RF algorithm evaluated feature importance by Gini coefficient reduction; the model error plateaued when the number of decision trees reached 500 (Figure. 5d), and the top 10 feature genes were selected according to the mean decrease in the Gini coefficient (Figure. 5e). For LASSO regression, the optimal regularization parameter λ was determined by inspecting the coefficient trajectory curve and cross-validation error curve (Figure. 5f–g). Venn diagram analysis of the feature genes obtained from the three machine learning algorithms identified six overlapping core feature genes: HSP90AA1, PRKCB, GRM3, AR, UBE2D3, and TERT (Figure. 5h). Using these six core feature genes, a PD risk scoring model was built to visualize the differences in the distribution of disease risk probabilities between healthy controls and patients with PD (Figure. 5i).

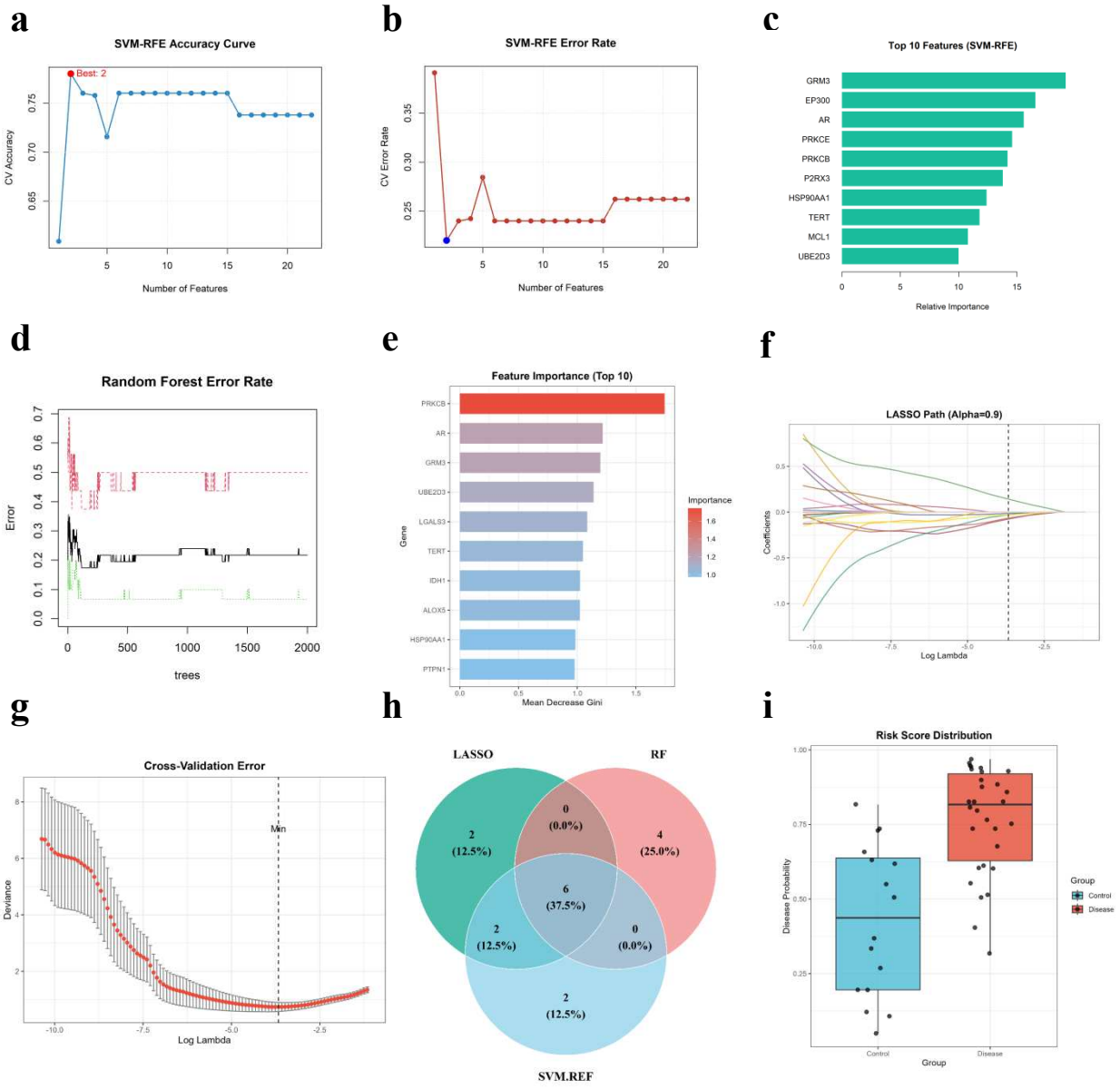


Figure 5. Screening of PD feature genes by multiple machine learning algorithms and risk score distribution

(a) Cross-validation accuracy curve of SVM-RFE; (b) Cross-validation error curve of SVM-RFE; (c) Bar plot showing importance of the top 10 SVM-RFE feature genes; (d) Error curve of random forest with increasing decision trees; (e) Top 10 core genes of random forest based on the mean decrease in the Gini coefficient; (f) Coefficient trajectory plot of LASSO regression; (g) Cross-validation error curve of LASSO regression; (h) Venn diagram of overlapping feature genes from LASSO, RF and SVM-RFE; (i) Box-and-whisker plot of risk scores in healthy controls and PD patients

3.5 External Validation of Core Targets Using the GSE7621 Dataset

The independent GSE7621 clinical dataset was used to externally validate the six machine-learning-identified core targets. Box-and-whisker plots revealed that only HSP90AA1 was significantly upregulated in PD patients versus healthy controls (P = 0.0015); no significant intergroup differences were found for the other five targets. One outlier existed in GRM3 expression of the PD group but did not alter the overall expression trend or affect intergroup difference assessment (Figure. 6a). ROC analysis (Figure. 6b,c) showed AUC values >0.5 for all six targets. HSP90AA1 had the best diagnostic performance (AUC = 0.833, 95% CI: 0.673–0.994), followed by AR (AUC = 0.688), UBE2D3 (AUC=0.667), GRM3 (AUC= 0.653), and PRKCB (AUC = 0.611) with declining discriminatory power; TERT exhibited the lowest performance (AUC=0.542). Collectively, HSP90AA1 outperformed other targets and may serve as a candidate diagnostic biomarker distinguishing PD patients from healthy controls. Transcriptomic data only reflect mRNA levels, while kinase activation depends mainly on post-translational phosphorylation. Since this mechanism is independent of transcriptional changes and transcriptomic data cannot capture protein phosphorylation, we further detected total protein and phosphorylation levels of PRKCB and STAT3 in animal models.

Combining machine-learning-derived feature genes and PPI network core nodes, we found HSP90AA1, PRKCB, and STAT3 potentially associate with the Nrf2 antioxidant pathway, supporting subsequent molecular simulation and in vivo validation.

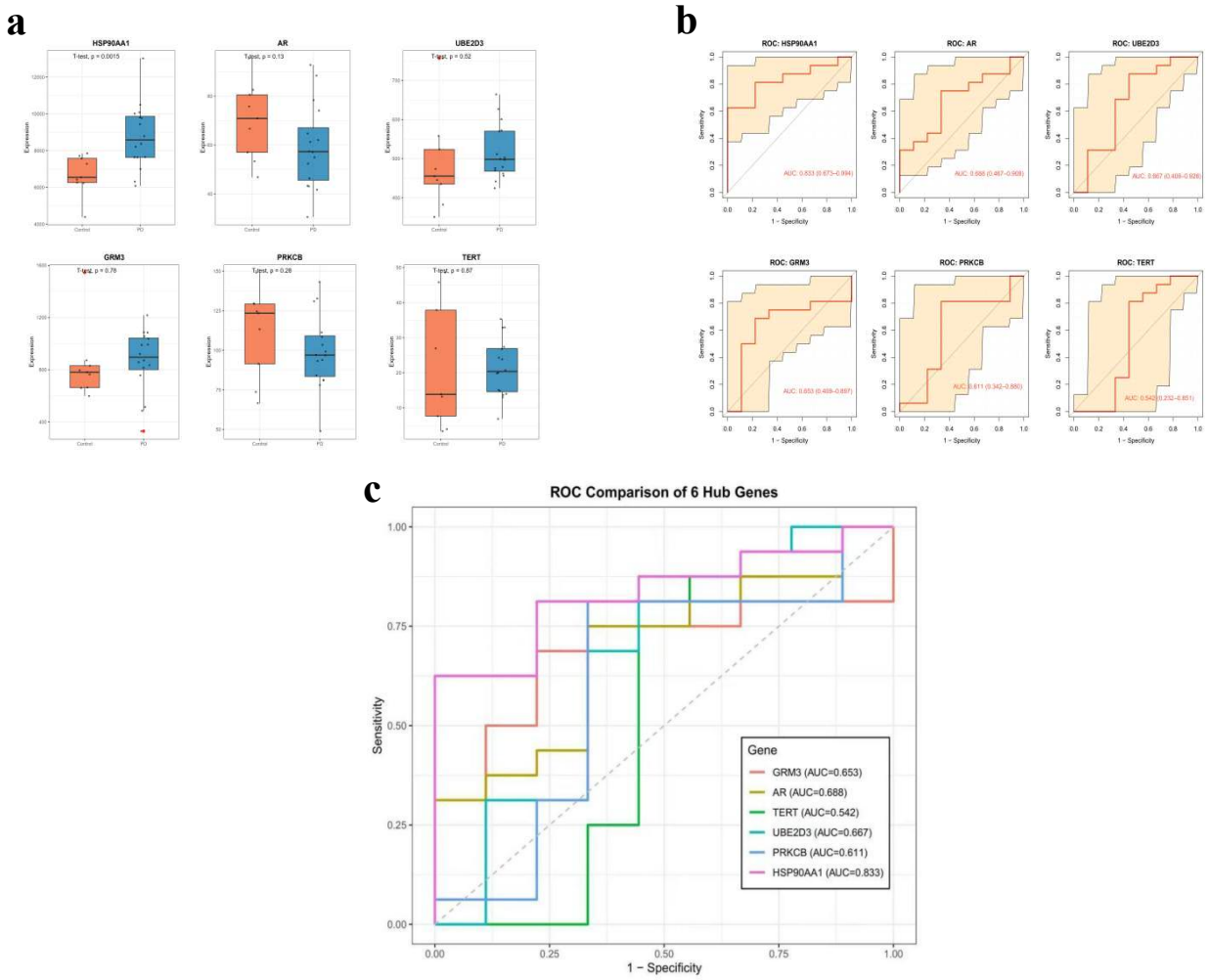
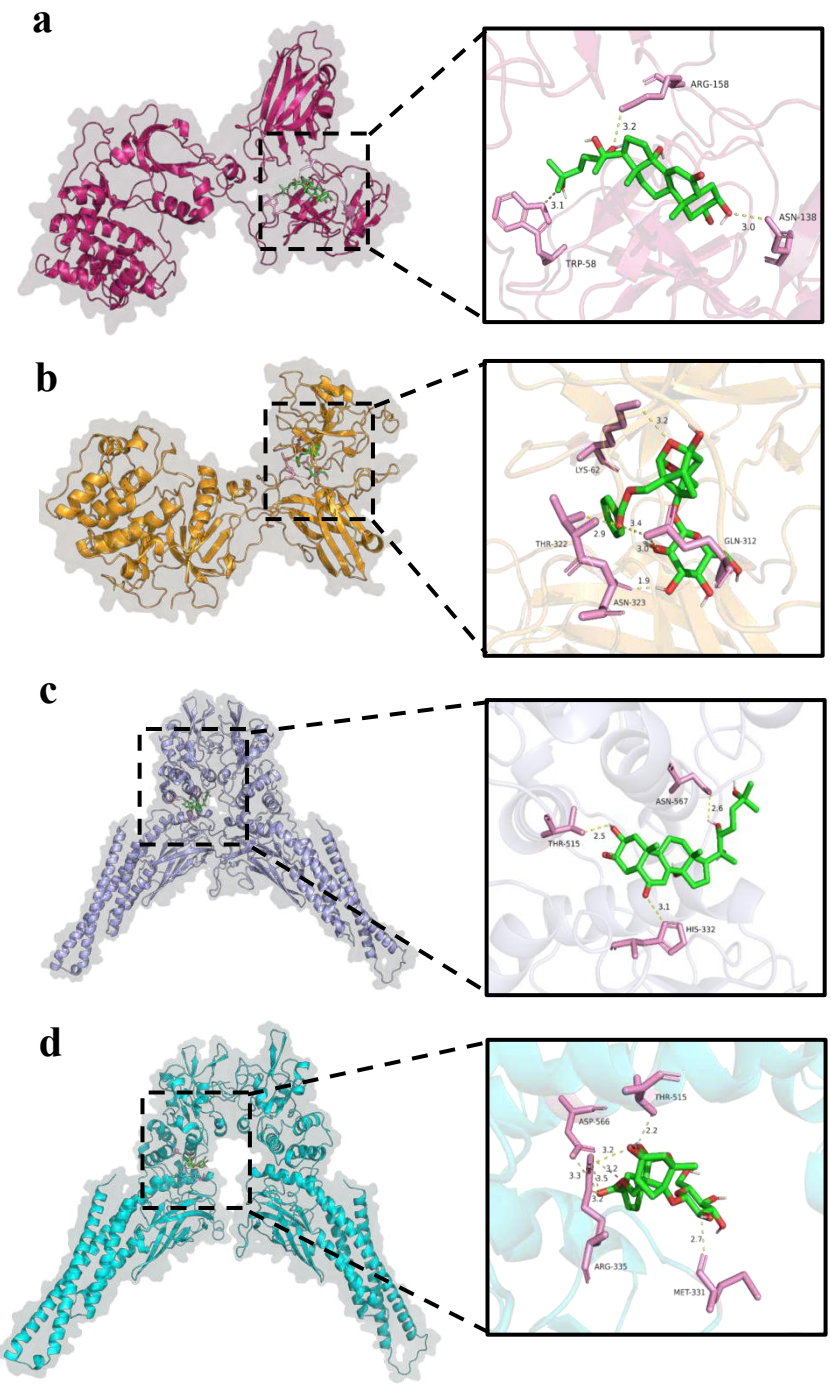


Figure 6. Validation of core target expression and diagnostic performance using the GSE7621 dataset

(a) Box plot showing target expression levels in the GSE7621 dataset; (b) Individual ROC curves for the six core genes; (c) Overlaid ROC plot comparing the six ROC curves

3.6 Validation of Molecular Docking for Active Ingredients and Key Targets

Molecular docking was performed for β-Ecd, PF and three key targets (PRKCB, STAT3, and HSP90AA1) to visualize 3D binding conformations and amino acid interactions (Figure.7a–f). All ligand–receptor complexes exhibited binding free energies < −5 kcal/mol, indicating spontaneous stable binding. The binding affinities of β-Ecd and PF to PRKCB were −7.8 and −7.9 kcal/mol; those to STAT3 were −8.1 and −8.2 kcal/mol; those to HSP90AA1 were −7.4 and −6.9 kcal/mol, showing the strongest binding to STAT3. These findings demonstrate that β-Ecd and PF directly bind PRKCB, STAT3, and HSP90AA1, providing a potential molecular basis for the regulation of PD-associated oxidative stress targets by the two compounds.


a
ARG-158
3.2
3.1
3.0
ASN-138
TRP-58
b
3.2
LYS-62
3.4
2.9
THR-322
GLN-312
1.9
ASN-323
c
ASN-567
2.6
THR-515
2.5
3.1
HIS-332
d
THR-515
ASP-566
2.2
3.2
3.2
3.5
ARG-335
MET-331

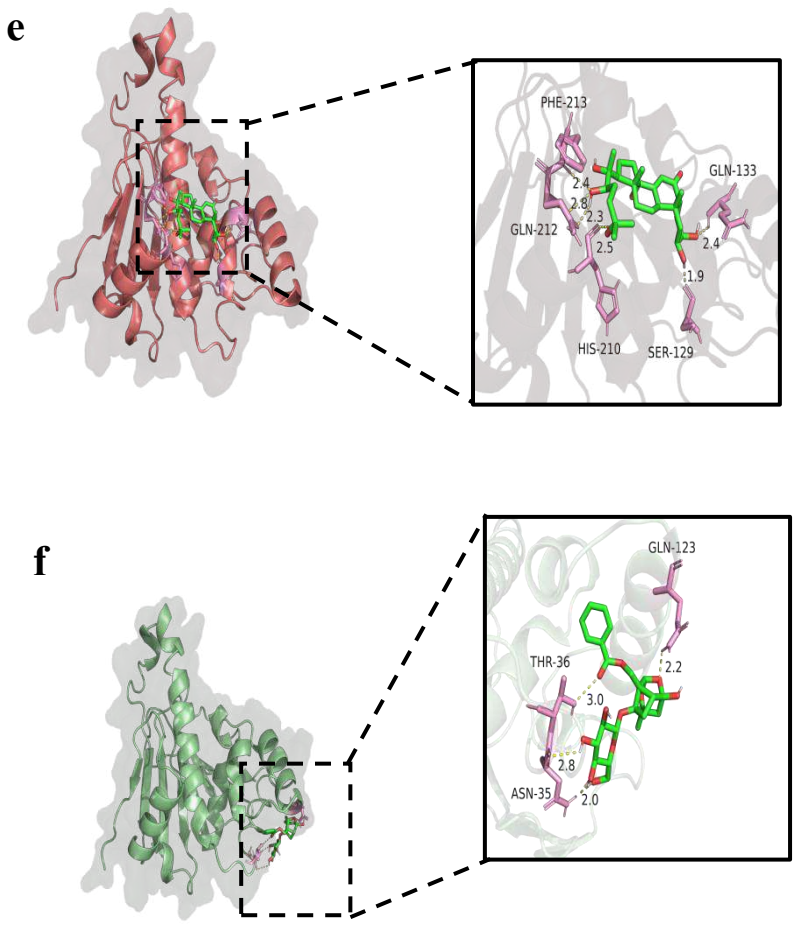


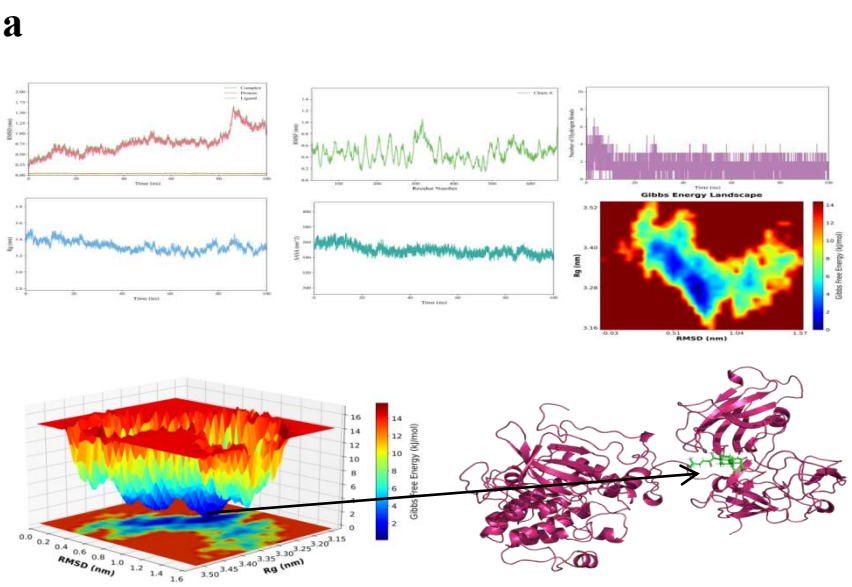
Figure 7. Molecular docking of active compounds with key targets

(a) Molecular docking of β-Ecd to PRKCB; (b) Molecular docking of PF to PRKCB; (c)Molecular docking of β-Ecd to STAT3; (d) Molecular docking of PF to STAT3; (e) Molecular docking of β-Ecd to HSP90AA1; (f) Molecular docking of PF to HSP90AA1

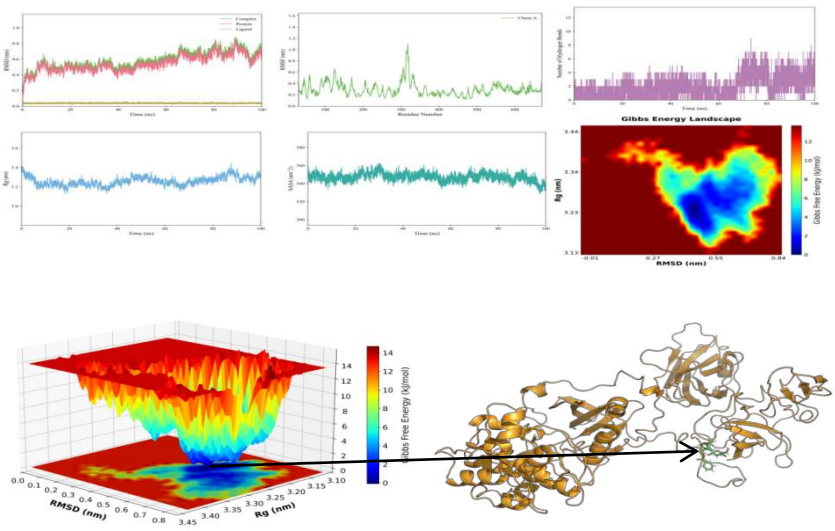
3.7 Validation of Molecular Dynamics Stability of Active Ingredient–Target Complexes

To verify the binding stability of β-Ecd and PF to core targets PRKCB, STAT3, and HSP90AA1, 100-ns molecular dynamics simulations were performed. RMSD analysis of the complexes was used to assess conformational dynamics of the whole simulation system. RMSD curves of all systems converged rapidly at the early simulation stage and maintained steady fluctuations thereafter without obvious conformational shifts, demonstrating that β-Ecd and PF form stable binding complexes with PRKCB, STAT3, and HSP90AA1, respectively. Root-mean-square fluctuation (RMSF) results revealed reduced flexibility of amino acid residues within the ligand-binding pocket, indicating that the small

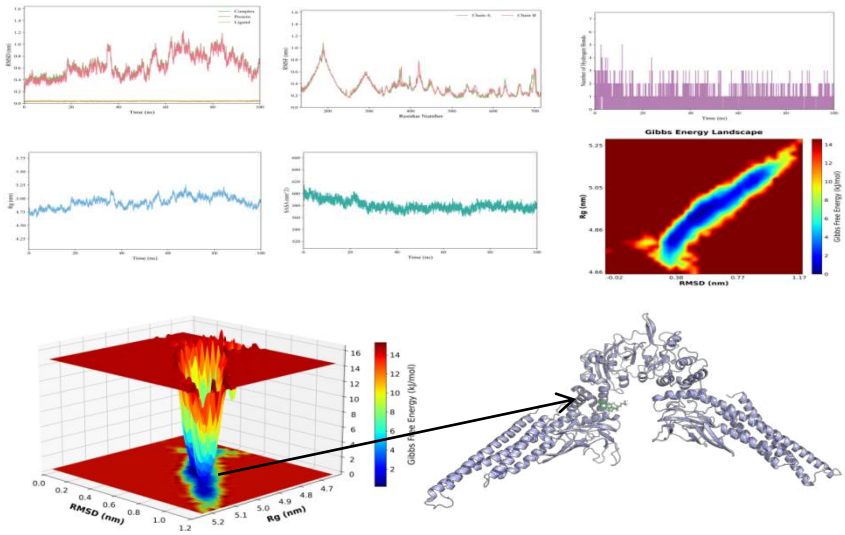
molecules form stable intermolecular interactions with the target active cavity and effectively restrict the movement of binding-site residues. Statistics of hydrogen bond counts during simulation showed persistent stable intermolecular hydrogen bonding, which supports stable complex binding. The radius of gyration (Rg) curve fluctuated steadily across the simulation without remarkable sustained changes, suggesting that the overall structures of PRKCB, STAT3, and HSP90AA1 remained compact; ligand binding did not induce protein denaturation or structural loosening. The solvent-accessible surface area (SASA) curve exhibited slight fluctuations throughout the simulation, showing that the ligand embeds inside the protein cavity, decreases exposure of hydrophobic regions, and further confirms tight ligand–protein binding. Two- and three-dimensional free energy landscapes (FEL) were constructed using RMSD and Rg. Each complex displayed one predominant low-energy conformation, confirming the thermodynamic stability of this binding mode. The 3D equilibrium conformations showed that β-Ecd and PF are stably accommodated within the active pockets of PRKCB, STAT3, and HSP90AA1, indicating stable binding between the active compounds and targets (Figure. 8a–f).



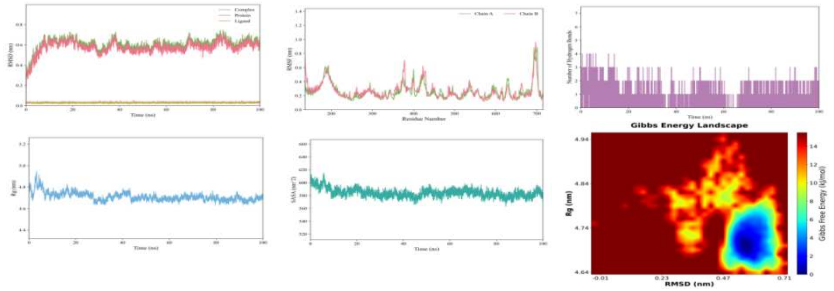
b

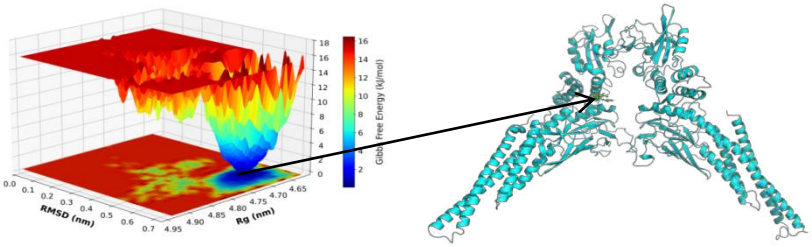

Gibbs Energy Landscape
RMSD (nm)
Rg (nm)
Gibbs Free Energy (kJ/mol)

c


Gibbs Energy Landscape
RMSD (nm)
Rg (nm)
Gibbs Free Energy (kJ/mol)

d


Gibbs Energy Landscape
RMSD (nm)
Rg (nm)
Gibbs Free Energy (kJ/mol)


RMSD (nm)
Rg (nm)
Gibbs Free Energy (kJ/mol)

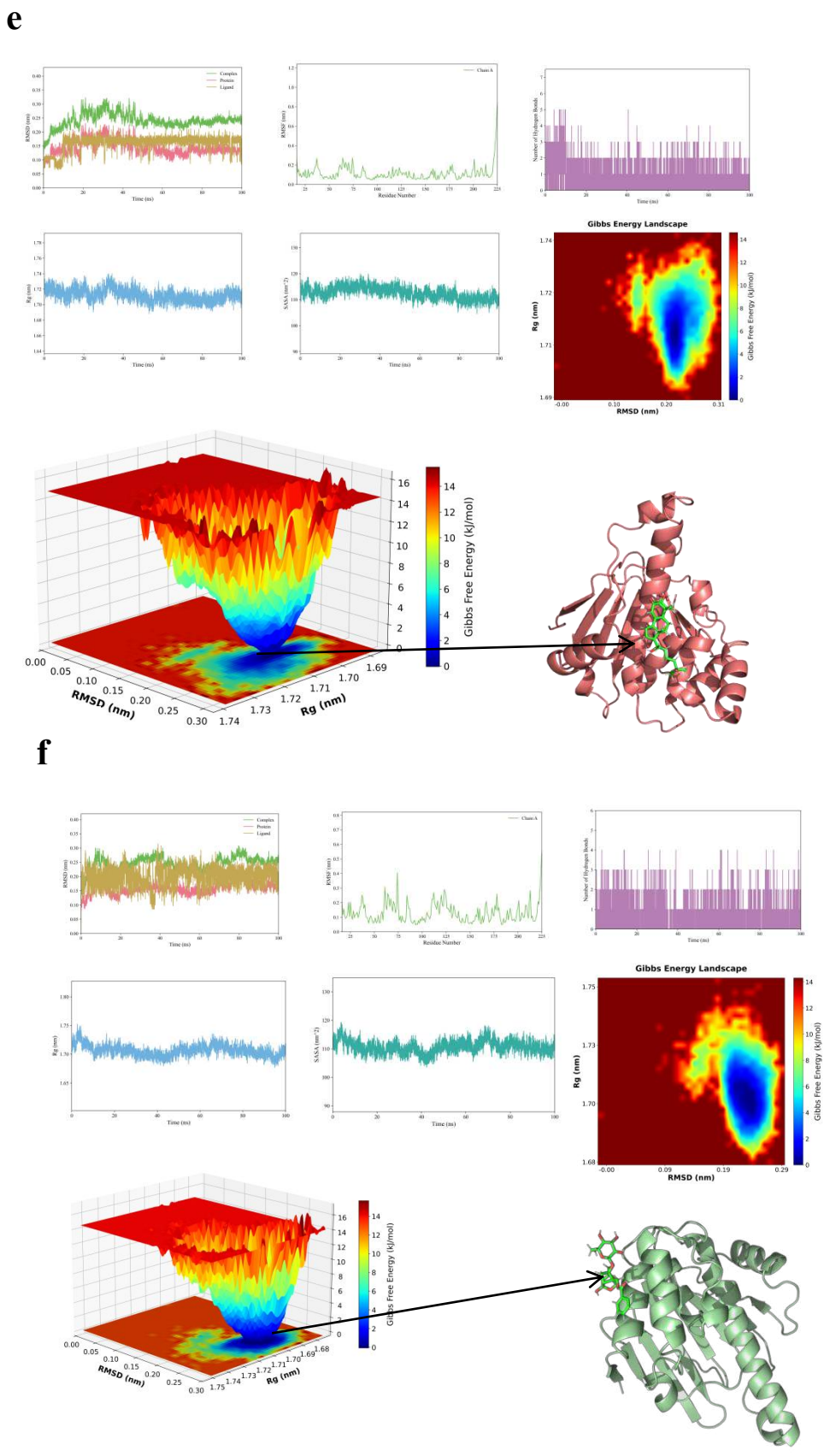


Figure 8. Stability analysis of 100 ns molecular dynamics simulations for β-Ecd and PF complexes with PRKCB, STAT3, and HSP90AA1

(a) β-Ecd–PRKCB complex; (b) PF–PRKCB complex; (c) β-Ecd–STAT3 complex; (d) PF–STAT3 complex; (e) β-Ecd–HSP90AA1 complex; (f) PF–HSP90AA1 complex

3.8 Effects of combined β-Ecd and PF treatment on muscular strength and balance function in PD mice

Behavioral evaluations comprising the pole-climbing and rotarod assays uncovered prominent motor impairments in PD model animals. Versus control mice, PD subjects required markedly prolonged pole-climbing latency, accompanied by a striking reduction in rotarod duration. When contrasted with the model cohort, co-administration of β-Ecd and PF curtailed pole-climbing latency and extended rotarod residence time. Importantly, this ameliorative capacity surpassed the outcomes achieved via separate monotherapies and was comparable to that of the positive control Sel(Table 3).

Table 3 Comparison of behavioral performance across mouse groups（$\bar{X}\pm S$，n=10）

Groups	Dose（mg/kg）	Pole climbing score	Rotarod duration/s
Control	0	0.10±0.32	289.90±11.28
MPTP	30	2.63±0.40$^{\#\#\#\#}$	43.00±27.45$^{\#\#\#\#}$
Sel	10	1.30±0.46***	192.70±55.79****
β-Ecd	2	2.07±0.47	138.80±61.95*
PF	20	1.90±0.47	131.20±46.76**
β-Ecd+PF	2:20	1.57±0.52*	179.80±62.16***

Data are reported as mean ± SD, with n = 10. $^{\#\#\#\#}P < 0.0001$ compared to the control group; $^{*}P < 0.05$,$^{**}P < 0.01$, $^{***}P < 0.001$, $^{****}P < 0.0001$ compared to the model group. The pole test was assessed with the Kruskal–Wallis H test, followed by Dunn's test and the Mann–Whitney U test. The rotarod test was analyzed using Welch's ANOVA and Welch's t-test.

3.9 Effects of combined β-Ecd and PF intervention on open-field behavioral performance in PD mice

Open-field behavioral assays were performed to assess locomotor and exploratory capacities of experimental mice (Figure. 9a). Compared with control animals, PD model animals displayed markedly shortened total travel distances and prolonged immobility durations (Figure.9b–c). Versus the model cohort, combinatorial administration of β-Ecd and PF effectively increased total travel distances and shortened immobility time in PD mice. Such behavioral ameliorative capacity surpassed the outcomes achieved via separate monotherapies and was comparable to that of the positive control selegiline (Sel), indicating that this combined pharmacological intervention prominently rescues impaired spontaneous locomotor activity in PD model mice.

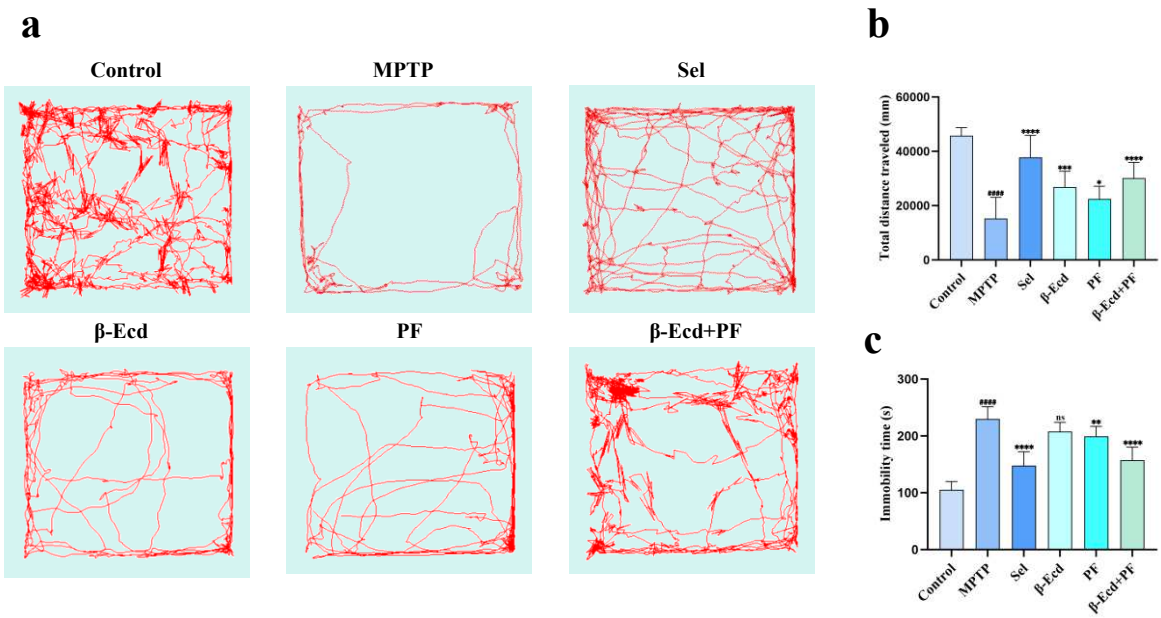


Figure 9. Behavioral performance of experimental mice

(a) Movement trajectory diagram; **(b)** Total travel distance; **(c)** Rotarod duration.

Data are expressed as mean ± SD, with $n = 10$. Statistical significance is indicated as $^{\#\#\#\#}P < 0.0001$ compared to the control group and as $^{*}P < 0.05$, $^{**}P < 0.01$, $^{***}P < 0.001$, $^{****}P < 0.0001$ (ns, not significant) compared to the model group. Statistical analyses were performed using one-way ANOVA, Dunnett's multiple comparison test and independent samples *t*-test.

3.10 Effects of β-Ecd combined with PF on neurodegeneration in PD mice

HE, Nissl and TH immunohistochemical assessments demonstrated evident morphological differences among groups. Relative to the control group, DA neurons within the SN of model mice presented disordered, dispersed arrangements alongside soma shrinkage and obscure nuclei. Nissl bodies displayed vague outlines, irregular loose distribution and distorted structures. Consistently, the model group possessed far fewer TH-positive neurons in the SN region. In contrast, treatment with combined β-Ecd and PF mitigated neuronal morphological defects and cellular damage (Figure.10a–d). Western blot analysis indicated suppressed TH protein abundance in model mice relative to control mice. Relative to the model cohort, such downregulation was substantially rescued following combination administration. Furthermore, the ameliorative effect of this combinatorial regimen was superior to that of single-agent treatment and comparable to that of the positive control Sel(Figure.10e–f).

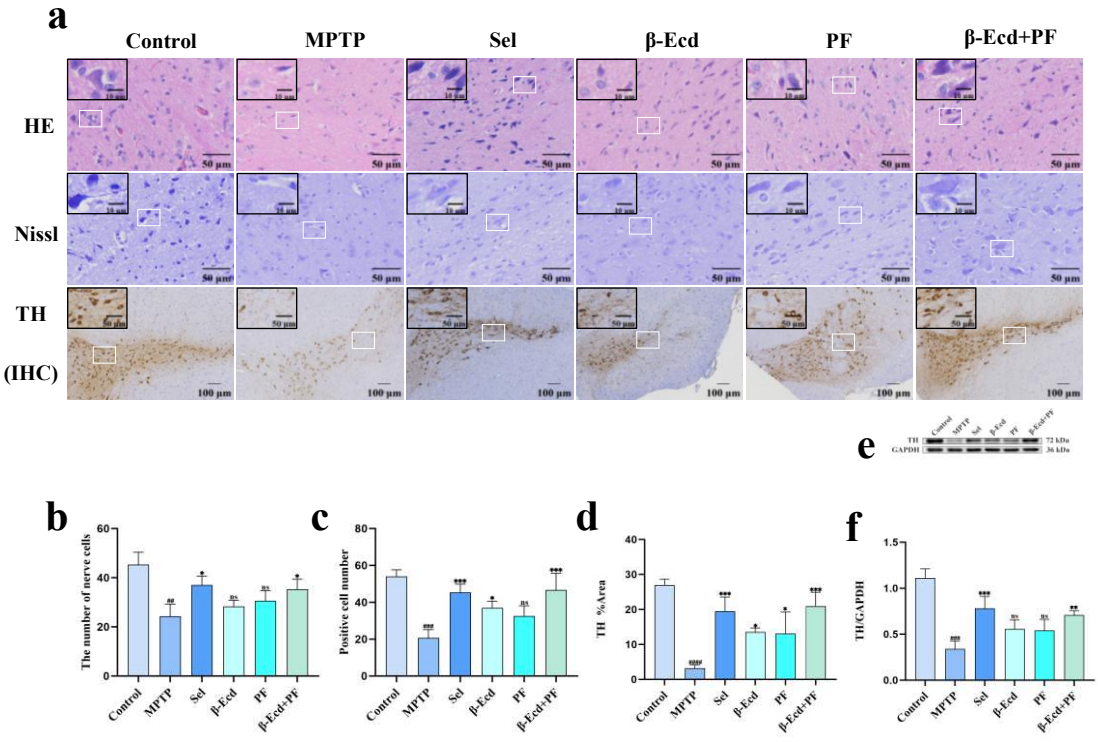


Figure 10.Combined β-Ecd and PF attenuates DA degeneration in the SN of PD mice.

(a) Evaluation of HE, Nissl and TH immunohistochemical staining in SN tissues. **(b–d)** Quantitative analysis of Nissl-positive neurons, TH-positive neurons and TH-positive area. **(e)** WB analysis for TH protein. **(f)** Densitometric analysis for relative TH expression. Data are expressed as mean ± SD, with n = 3. Statistical significance is indicated as $^{\#\#}P < 0.01$, $^{\#\#\#}P < 0.001$, $^{\#\#\#\#}P < 0.0001$ compared to the control group and as $^{*}P < 0.05$,$^{**}P < 0.01$, $^{***}P< 0.001$ (ns, not

significant) compared to the model group.One-way ANOVA was applied, followed by Dunnett's test and independent t-test for statistical comparisons.

3.11 Effects of β-Ecd Combined with PF on DAT Protein Expression in the Midbrain of PD Mice

As an essential protein localized at the presynaptic membrane of DA neurons, DAT can reflect the functional condition and survival status of these neurons. WB outcomes revealed markedly diminished DAT abundance in the model group relative to the control group, indicative of impaired neuronal function. Compared with the model group, co-administration of β-Ecd and PF elevated DAT levels. The combinatorial regimen exerted superior beneficial effects to single-agent treatment, with efficacy comparable to that of the positive control Sel.(Figure. 11a–b).

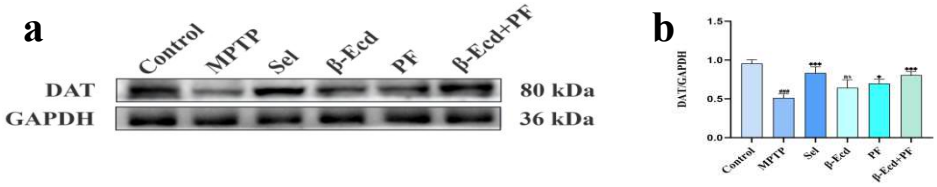


Figure 11. Combined β-Ecd and PF modulate DAT expression in the midbrain of PD mice.

(a) Evaluation of DAT protein via WB analysis. **(b)** Densitometric analysis for relative DAT expression. Data are expressed as mean ± SD, with n = 3. Statistical significance is indicated as $^{###}P < 0.001$ compared to the control group and as $^{*}P < 0.05$, $^{***}P < 0.001$ (ns, not significant) compared to the model group. One-way ANOVA was applied, followed by Dunnett's test and independent t-test for statistical comparisons.

3.12 Effects of β-Ecd Combined with PF on Oxidative Stress Markers in the Midbrain of PD Mice

An oxidative stress detection kit coupled with a visible spectrophotometer was used to assess the effects of β-Ecd and PF co-administration on CAT, SOD and total antioxidant capacity (T-AOC) levels. Experimental data revealed that CAT and SOD enzymatic activities as well as T-AOC were markedly decreased in the model group relative to the control group. In comparison with the model group, the combinatorial regimen effectively elevated these antioxidant markers and relieved oxidative stress injury, and its efficacy was significantly superior to that of single-agent treatment (Figure. 12a–c).

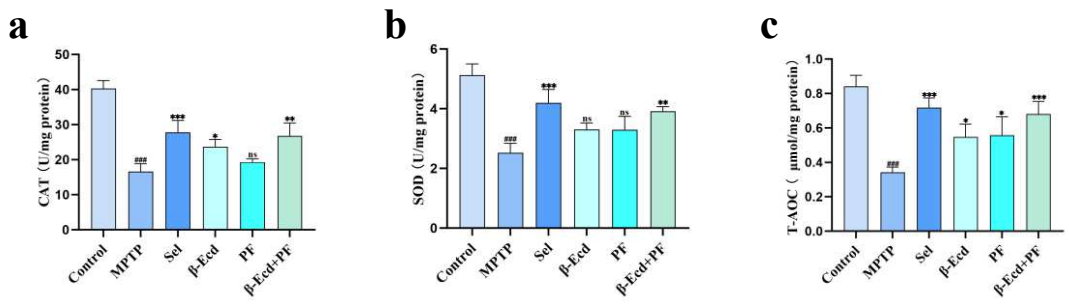


Figure 12. Combined β-Ecd and PF modulate midbrain oxidative stress markers in PD mice.

(a) Quantitative analysis of CAT activity. **(b)** Quantitative analysis of SOD activity.**(c)** Quantitative analysis of T-AOC levels.

Data are expressed as mean ± SD, with n = 3. Statistical significance is indicated as $^{###}P < 0.001$ compared to the control group and as $^{*}P < 0.05$, $^{**}P < 0.01$, $^{***}P < 0.001$ (ns, not significant) compared to the model group. One-way ANOVA was applied, followed by Dunnett's test and independent t-test for statistical comparisons.

3.13 Effects of β-Ecd combined with PF on the phosphorylation of PRKCB, STAT3 and HSP90AA1 protein expression in the midbrain of PD mice

Western blot outcomes revealed no significant differences in the total protein expression of PRKCB and STAT3 between the control group and the model group. The ratios of p-PRKCB/PRKCB and p-STAT3/STAT3 were markedly elevated, accompanied by significant upregulation of HSP90AA1 protein abundance in the model group relative to the control group. Relative to the model cohort, combinatorial administration of β-Ecd and PF prominently reduced the p-PRKCB/PRKCB and p-STAT3/STAT3 phosphorylation ratios and downregulated HSP90AA1 expression. This ameliorative effect surpassed the outcomes achieved via separate monotherapies and was comparable to that of the positive control Sel (Figure.13a–d).

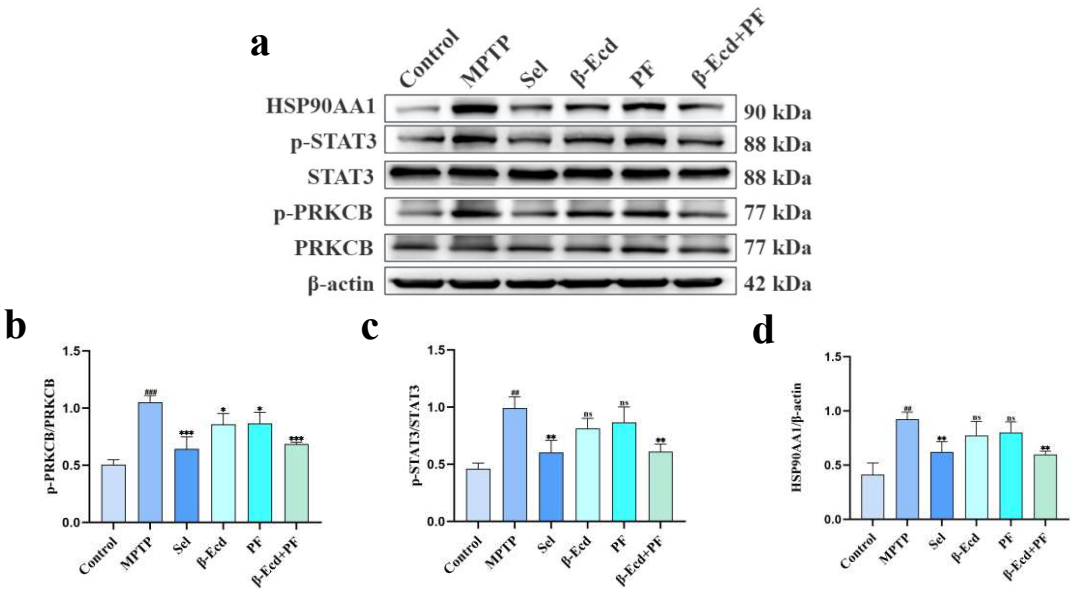


Figure 13. Combined β-Ecd and PF affect PRKCB, STAT3 phosphorylation and HSP90AA1 protein expression in the midbrain of PD mice.

(a) Western blot bands of p-PRKCB, PRKCB, p-STAT3, STAT3, HSP90AA1 and β-actin in the midbrain of mice from each group. **(b–d)** Quantitative analysis of p-PRKCB/PRKCB, p-STAT3/STAT3 phosphorylation ratios and the relative expression level of HSP90AA1 protein.

Data are expressed as mean ± SD, with n = 3. Statistical significance is indicated as $^{\#\#}P < 0.01$, $^{\#\#\#}P < 0.001$ compared to the control group and as $^{*}P < 0.05$, $^{**}P < 0.01$, $^{***}P < 0.001$ (ns, not significant) compared to the model group. One-way ANOVA was applied, followed by Dunnett's multiple comparisons test and independent t-test for statistical comparisons.

3.14 Effects of β-Ecd Combined with PF on Nrf2-Mediated Antioxidant Pathways in the Midbrain of PD Mice

WB results demonstrated that the abundances of Nrf2, HO-1 and NQO-1 markedly declined in the model group compared with the control group. Relative to the model group, co-administration of β-Ecd and PF markedly upregulated the protein levels of Nrf2, HO-1 and NQO-1. The combinatorial regimen exerted ameliorative effects superior to that of single-agent treatment (Figure. 14a–d).

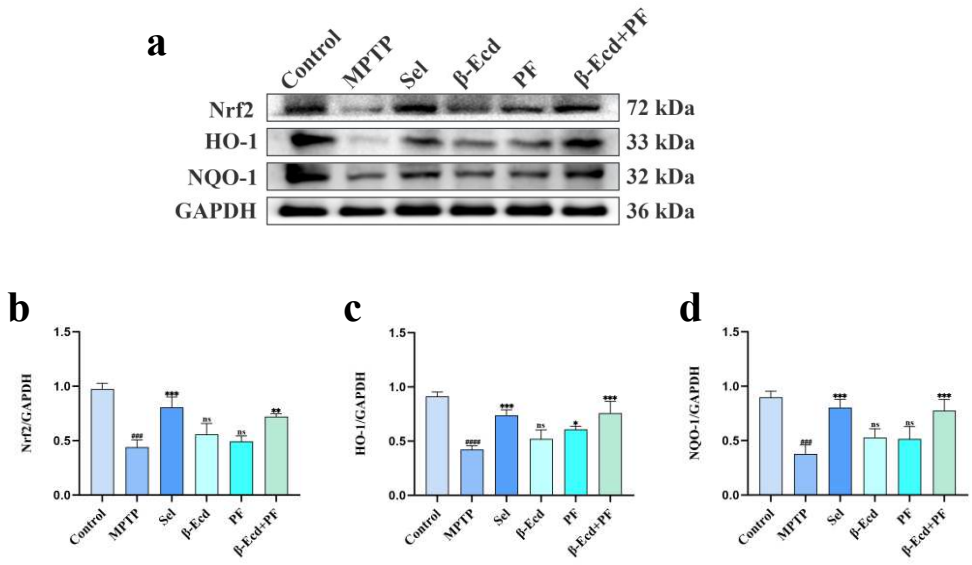


Figure 14. Combined β-Ecd and PF regulation of Nrf2, HO-1, NQO1 in PD mice.

(a) WB analysis illustrating expression levels of Nrf2, HO-1, NQO1, andGAPDH. **(b)** Densitometric evaluation detailing relative Nrf2 expression. **(c)** Densitometric analysis for relative HO-1 expression. **(d)** Densitometric assessment concerning relative NQO1 expression. Results are expressed as mean ± SD, for n = 3, with $^{\#\#\#\#}P < 0.0001$, $^{\#\#\#}P < 0.001$ indicating a significant difference from the control and $^{*}P < 0.05$, $^{**}P < 0.01$ and $^{***}P < 0.001$ (ns, not significant)compared to the model group. One-way ANOVA was applied, followed by Dunnett's test and independent t-test for statistical comparisons.

3.15 Co-administration of β-Ecd and PF modulates Bcl-2 and BAX expression to suppress neuronal apoptosis

Western blot findings indicated that the model group displayed reduced Bcl-2 abundance and elevated BAX expression compared with the control group. Compared with the model group, concurrent treatment with β-Ecd and PF significantly increased Bcl-2 levels while lowering BAX expression. These observations demonstrate that this two-agent intervention inhibits aberrant midbrain neuronal apoptosis by regulating apoptosis-associated proteins. This ameliorative effect surpassed the outcomes achieved via single-agent treatment and was comparable to that of the positive control Sel, conferring neuroprotective effects (Figure 15.a–c).

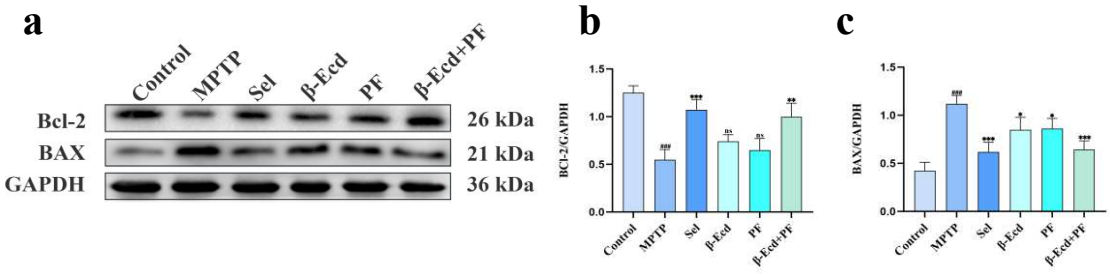


Figure 15. Combined β-Ecd and PF modulate Bcl-2 and BAX in PD mice.

(a) Western blot analysis illustrating expression levels of Bcl-2, BAX and GAPDH. **(b)** Densitometric evaluation detailing relative Bcl-2 expression. **(c)** Densitometric analysis for relative BAX expression. Results are expressed as mean ± SD, for n = 3, with $^{\#\#\#}P < 0.001$ indicating a significant difference from the control and $^{*}P < 0.05$, $^{**}P < 0.01$ and $^{***}P < 0.001$ signifying statistical significance compared to the Model group; ns denotes no significant difference. One-way ANOVA was applied, followed by Dunnett's test and independent t-test for statistical comparisons.

4.Discussion

Current PD clinical therapies have notable limitations and cannot halt disease progression. Accordingly, exploring PD pathogenesis and developing safe, effective agents remain key research priorities. As core active constituents of Achyranthes bidentata and Paeonia lactiflora, β-Ecd and PF exert potent antioxidant, anti-inflammatory and neuroprotective effects. Liu et al. established a rotenone-induced PC12 cell PD model and showed rotenone elevates intracellular ROS and triggers neuronal injury; combined PF and β-Ecd treatment produces synergistic protection and relieves rotenone-induced cellular damage[18]. Rong et al. demonstrated in a chronic MPTP mouse PD model that β-Ecd alleviates midbrain oxidative injury, protects TH-positive dopaminergic neurons and improves motor performance[10]. Rong Hua et al. reported PF ameliorates motor dysfunction in MPTP-treated mice, suppresses substantia nigra dopaminergic neuronal apoptosis, reduces caspase-3 activity and downregulates α-Syn expression to exert neuroprotection[19]. Previous studies mainly report individual protective effects of β-Ecd or PF against PD, while the mechanisms underlying their combined anti-PD effects remain largely uncharacterized. To our knowledge, no in vivo PD studies have examined whether this combination modulates HSP90AA1, PRKCB, and STAT3 to regulate the

Nrf2-mediated oxidative stress pathway. Herein, we identified these three core candidate targets via multi-algorithm machine learning screening, consistent with prior reports linking them to Nrf2 pathway regulation [20–23]. We investigated whether combined β-Ecd and PF act on the Nrf2 pathway by regulating these upstream targets to validate their neuroprotective activity. This work explores the association between target modulation by the β-Ecd/PF combination and the Nrf2-dependent oxidative stress pathway, clarifying how these compounds mitigate PD pathological injury and supplying experimental evidence for their use in PD prevention and treatment.

Virtual predictions based on public databases can identify potential targets of traditional Chinese medicine active ingredients for PD intervention and support the generation of testable hypotheses. This study adopted network pharmacology, multi-algorithm machine learning and molecular dynamics simulations for target screening to elucidate the molecular mechanism underlying combined therapy against PD. The core active ingredients of this herbal pair, β-Ecd and PF, were screened from the TCMSP database. PD-related differentially expressed genes were retrieved from GEO transcriptomic datasets. Integrating multi-database predictions, we obtained common drug–disease targets to build a reliable dataset for mechanistic exploration. PPI network construction combined with GO and KEGG enrichment analyses revealed that oxidative stress response was the core biological process, with marked enrichment of oxidative-stress-related pathways including JAK–STAT. To overcome the bias from a single screening method, we combined PPI topological analysis with machine learning algorithms and identified Nrf2 pathway-associated STAT3, HSP90AA1 and PRKCB as core validation targets. Three algorithms (LASSO regression, random forest and SVM-RFE) were used for cross-screening, yielding six candidate targets at the intersection. Combined with enrichment results and published literature, PRKCB and STAT3 act as upstream regulators of the Nrf2 antioxidant pathway, and HSP90AA1 modulates their protein stability and activity via chaperone function. Owing to their tight correlation with oxidative stress, the three molecules were selected as core candidates. Molecular docking and 100 ns MD simulations confirmed stable binding of β-Ecd and PF to these three targets. External validation using the GSE7621 dataset showed that only HSP90AA1 was significantly upregulated in PD patient tissues (P = 0.0015), with optimal diagnostic performance

(AUC = 0.833, 95% CI: 0.673–0.994). Notably, this diagnostic model was built on human public transcriptomic data. Although we verified altered HSP90AA1 protein expression in animal models, the model has not been validated in mouse samples, indicating HSP90AA1 as a promising clinical biomarker for PD. Integrating network pharmacology, machine learning screening, molecular docking and MD simulations, we propose that HSP90AA1, PRKCB and STAT3 serve as core targets for β-Ecd combined with PF to treat PD. GSE7621 validation revealed intergroup mRNA differences only in HSP90AA1, while PRKCB mRNA showed no statistical difference. This implies PRKCB regulation occurs at the post-translational phosphorylation level. Transcriptomics only reflects transcriptional abundance and cannot capture protein post-translational modifications, which supports our detection of PRKCB and STAT3 phosphorylation in animal models. Based on these in silico findings, we proposed our hypothesis and validated it using an MPTP-induced PD mouse model.

PD is mainly characterized by dopaminergic neuronal degeneration in the substantia nigra (SN) of the midbrain. Motor dysfunction represents its typical clinical manifestation, and oxidative stress imbalance serves as a core mechanism driving neuronal injury and subsequent motor impairment[24]. MPTP is extensively applied to establish animal models recapitulating PD-like phenotypes and symptoms, and it remains one of the most commonly adopted PD animal models[25–27]. To verify the hypothesized protective effect of combined β-Ecd and PF against PD, we constructed an MPTP-induced PD mouse model. Behavioral tests revealed that model mice exhibited a significantly longer pole-climbing time and shorter rotarod endurance time. In the open-field test, these mice showed decreased total travel distance and extended immobility time, indicating disturbed muscle balance and impaired motor coordination. By contrast, combined β-Ecd and PF treatment markedly rescued the above motor deficits in PD model mice. These behavioral findings confirm that the β-Ecd/PF combination ameliorates motor dysfunction in PD model mice. Nevertheless, whether this improvement arises from alleviated damage to mesostriatal DA neurons requires further histopathological validation.

The progressive degeneration and loss of dopaminergic neurons in the substantia nigra pars compacta constitutes the

core pathological mechanism underlying motor abnormalities in PD. To elucidate the neuroprotective effects of combined β-Ecd and PF on dopaminergic neurons, multiple histological stains were applied to assess neuronal injury comprehensively. Progressive loss of midbrain nigral dopaminergic neurons and somal morphological abnormalities are hallmark pathological changes of PD[28]. Hematoxylin and eosin (HE) staining visualizes neuronal morphology and tissue architecture; Nissl staining evaluates ribosomal integrity within neuronal cytoplasm; TH acts as a specific marker for SN DA neurons. Combined use of these three staining methods allows comprehensive assessment of neuronal damage[29–31]. Herein, HE, Nissl and TH immunohistochemistry revealed disorganized tissue arrangement, somal atrophy and reduced viable neurons in the SN of PD mice. Combined β-Ecd and PF treatment attenuated neuronal injury, preserved cellular morphology and structural integrity, and increased TH-positive neuron counts. Meanwhile, this regimen reversed the downregulation of DAT protein in midbrain tissue, further supporting its DA neuroprotection. This protective effect exceeded monotherapy and was comparable to the positive control Sel.

The above morphological findings confirm that combined β-Ecd and PF alleviate degenerative injury of substantia nigra DA neurons, with oxidative stress imbalance as a critical driver of neuronal degeneration and death. Oxidative stress damages cell membranes and intracellular biomolecules, impairing neuronal function. Substantia nigra DA neurons are highly vulnerable to oxidative stress, and disrupted antioxidant homeostasis further aggravates neuronal injury[32]. Many studies have identified Nrf2 as a core regulator of cellular antioxidant responses[33]. Using machine learning, we screened three potential upstream targets: PRKCB, STAT3 and HSP90AA1, all reported to regulate the Nrf2 pathway. Wu et al. showed that PRKCB-encoded PKC acts as an upstream Nrf2 signaling regulator; aberrant PKC activation mediates synaptic oxidative damage in bisphenol A-treated HT22 cells [34]. In a thioacetamide-induced rat hepatocellular carcinoma model, El Far et al. validated that the versican/PDGF/PKC pathway negatively modulates Nrf2 antioxidant activity. Inhibiting this pathway restores Nrf2-dependent antioxidant function and mitigates oxidative injury[35]. Hassan et al. reported in squamous cell carcinoma models that STAT3 activates the STAT3/Nrf2 cascade to enhance cellular antioxidant capacity[36]. Prior PKC-family studies mainly focus on general PKC functions; systematic

in vivo evidence for phosphorylation regulation and drug responses of PRKCB-encoded PKCβ under PD pathology remains absent. Sun et al. demonstrated that neuroinflammatory stimulation induces PKCβ phosphorylation and activation in LPS-treated BV2 microglia, contributing to neuronal injury [37]. In an MPTP-induced subacute PD mouse model, Yang et al. found STAT3 activation depends on phosphorylation. Under PD pathology, p-STAT3 increases abnormally while total STAT3 stays unchanged; such aberrant activation disrupts Nrf2 homeostasis and mediates neuronal damage [38]. Using bleomycin-induced pulmonary fibrosis mice and A549 cell models, Shen et al. further revealed that HSP90AA1 interacts with STAT3 and modulates STAT3 phosphorylation and activation [39].

HSP90AA1, an essential chaperone protein, stabilizes the conformation of PRKCB and STAT3 and maintains their expression and activation levels. Under PD pathological conditions, upregulated HSP90AA1 may enhance the protein stability of PRKCB and STAT3 to indirectly promote their phosphorylation and activation, participating in the pathological regulation of oxidative stress in PD [23,39,40]. Combined with our machine learning screening results and published evidence, We propose the following scientific hypothesis: pathologically elevated HSP90AA1 in PD maintains the protein stability of PRKCB and STAT3 via its chaperone function, promotes their aberrant phosphorylation and activation, and subsequently suppresses the downstream Nrf2 antioxidant pathway, thereby aggravating oxidative stress injury of dopaminergic (DA) neurons in the substantia nigra. In contrast, combined β-Ecd and PF modulate the expression and activation levels of the above targets, restore Nrf2-mediated antioxidant homeostasis, and thereby alleviate MPTP-induced neuronal degenerative damage, suggesting that HSP90AA1, PRKCB and STAT3 may jointly participate in the pathological process of oxidative stress in PD.

Based on the above hypothesis, we systematically validated the neuroprotective effects of combined β-Ecd and PF by assessing oxidative stress indicators and molecular proteins. Experiments revealed that midbrain tissues from MPTP-induced PD mice exhibited reduced SOD and CAT activities, decreased T-AOC levels, and disrupted local antioxidant homeostasis. Combined β-Ecd and PF treatment strengthened tissue antioxidant defense and attenuated tissue injury, with effects comparable to the positive control Sel. Western blot (WB) results showed increased HSP90AA1 expression in PD mice. Although total PRKCB and STAT3 protein levels remained unchanged, elevated ratios of phosphorylated to total protein were observed for both proteins, indicating their excessive activation. These

observations are consistent with prior MPTP-model studies[16, 23, 34, 39]. Combination treatment downregulated aberrant HSP90AA1 expression, lowered p-PRKCB/PRKCB and pSTAT3/STAT3 ratios, and increased expression of the Nrf2/HO-1/NQO1 pathway; these protective effects were comparable to sel. Oxidative stress overload can trigger neuronal apoptosis. Analysis of apoptosis-associated proteins demonstrated that the combination regimen upregulated Bcl-2 and downregulated Bax, suggesting this drug combination modulates apoptotic molecules to mitigate oxidative stress-triggered neuronal apoptosis.

Taken together, combined β-Ecd and PF can downregulate the expression level of HSP90AA1 and inhibit the phosphorylation and activation levels of PRKCB and STAT3, thereby activating the Nrf2 antioxidant pathway together with its downstream HO-1 and NQO1.These molecular alterations correlate with improved motor performance, alleviated cerebral oxidative injury and substantia nigra DA neuroprotection, supporting the hypothesis raised herein. Furthermore, this combination concurrently modulates multiple targets and signaling pathways, yielding stronger neuroprotection than monotherapy, this regimen may exert neuroprotective effects via modulation of these candidate targets to activate the Nrf2 antioxidant cascade. Multi-algorithm machine learning is applied for target screening, enabling systematic exploration from virtual prediction to in vivo animal validation. The present work provides in silico prediction and in vivo experimental evidence for combined β-Ecd and PF in PD treatment and offers a reference for combinatorial studies of active components from traditional Chinese medicine. Notably, alterations in candidate targets and downstream molecular markers are detected solely within animal models. Functional assays including gene knockout and target inhibitor experiments remain absent; thus, the direct regulatory effects of HSP90AA1, PRKCB and STAT3 on the Nrf2 pathway cannot be confirmed. The precise regulatory relationship between these candidate targets and Nrf2 pathway activation awaits further investigation.

5.Conclusions:

This study integrated bioinformatics, machine learning prediction and molecular simulation, combined with an MPTP-induced PD mouse model, to explore the potential mechanism by which β-Ecd combined with PF modulates the Nrf2 pathway to ameliorate oxidative stress injury in PD. Molecular simulations confirmed stable binding of β-Ecd and PF to HSP90AA1, PRKCB and STAT3. In vivo animal experiments demonstrated that the combination of β-Ecd and PF improved motor performance, alleviated the damage of substantia nigra dopaminergic neurons, enhanced antioxidant capacity and suppressed neuronal apoptosis in PD mice, with superior effects compared with monotherapy. Mechanistically, this combined treatment downregulated HSP90AA1 expression, inhibited aberrant phosphorylation of PRKCB and STAT3, and subsequently activated the Nrf2 antioxidant pathway and its downstream HO-1 and NQO1, thereby relieving neuronal oxidative damage. This study provides experimental evidence supporting the material basis underlying the anti-Parkinsonian effects of β-Ecd combined with PF and offers insights for the development of natural

active agents for PD. Nevertheless, this work only validated phenotypic changes and protein expression at the animal level, and genetic knockout and pharmacological inhibitor interventions are still required to establish the causal relationship within the HSP90AA1-PRKCB-STAT3-Nrf2 ; further targeted intervention experiments will be performed to clarify this regulatory cascade.

Abbreviations

biological processes (BP)

cellular component (CC)

differentially expressed genes (DEGs)

dopaminergic (DA)

free energy landscapes (FEL)

Hematoxylin-eosin staining (HE)

Immunohistochemistry (IHC)

molecular dynamics (MD)

Molecular function (MF)

Parkinson's disease (PD)

paeoniflorin (PF)

phenylmethanesulfonyl fluoride (PMSF)

Principal component analysis (PCA)

protein-protein interaction (PPI)

polyvinylidene difluoride (PVDF)

Radio-immunoprecipitation assay (RIPA)

Random Forest (RF)

Radius of gyration (Rg)

reactive oxygen species (ROS)

Root-mean-square deviation (RMSD)

Root-mean-square fluctuation (RMSF)

selegiline (Sel)

sodium dodecyl sulfate-polyacrylamide gel electrophoresis (SDS-PAGE)

Solvent-accessible surface area (SASA)

substantia nigra (SN)

total antioxidant capacity (T-AOC)

Traditional Chinese Medicine Systems Pharmacology Database (TCMSP)

Western blot (WB)

β-Ecdysone (β-Ecd)

References

1.Tolosa, E.; Garrido, A.; Scholz, S.W.; Poewe, W. Challenges in the diagnosis of Parkinson's disease. Lancet Neurol. 2021, 20, 385–397.

2.Kulcsarova, K.; Skorvanek, M.; Postuma, R.B.; Berg, D. Defining Parkinson's Disease: Past and Future. J. Park. Dis. 2024, 14, S257–S271.

3.Trevisan, L.; Gaudio, A.; Monfrini, E.; Avanzino, L.; Di Fonzo, A.; Mandich, P. Genetics in Parkinson's disease, state-of-the-art and future perspectives. Br. Med. Bull. 2024, 149, 60–71.

4.Burton, M.; Marsden, D.; Harish, D.; Morris, P.; Heneghan, C.; Butler, A.; Nunan, D. Subcutaneous Levodopa in Parkinson's Disease: A Systematic Review and Meta-Analysis. Eur. J. Neurol. 2026, 33, e70506.

5.Aktaş, E.; Hanağası, H.A.; Özgentürk, N.Ö. Levodopa and Plant-Derived Bioactive Compounds in Parkinson's Disease: Mechanisms, Efficacy, and Future Perspectives. CNS Neurosci. Ther. 2025, 31, e70540.

6.Gao, Y.; Tang, X.; Yao, J.; Sun, T.; Chen, Y.; Cheng, C.; Yang, J.; Wang, B.; Liu, A.; Yang, L.; Zhao, M. Targeting the bile acid receptor TGR5 with Gentiopicroside to activate Nrf2 antioxidant signaling and mitigate Parkinson's disease in an MPTP mouse model. J. Adv. Res. 2026, 80, 977–990.

7.Jia, H.; Liu, M.; Jiang, H.; Qiao, Z.; Ren, K.; Du, X.; Chen, X.; Jiao, Q.; Che, F. Repurposing of epalrestat for neuroprotection in Parkinson's disease via activation of the KEAP1/Nrf2 pathway. J. Neuroinflammation. 2025, 22, 125.

8.Liu, X.; Zheng, Z.; Xue, C.; Wang, X.; Li, J.; Liu, Z.; Xin, W.; Xu, X.; Zhou, D.; Yao, L.; Lu, G. LRRK2 Mediates α-Synuclein-Induced Neuroinflammation and Ferroptosis through the p62-Keap1-Nrf2 Pathway in Parkinson's Disease. Inflammation 2025, 48, 3666–3691.

9.Vágvölgyi, M.; Laczkó, D.; Santa-Maria, A.R.; Vigh, J.P.; Walter, F.R.; Berkecz, R.; Deli, M.A.; Tóth, G.; Hunyadi, A. 17-Oxime ethers of oxidized ecdysteroid derivatives modulate oxidative stress in human brain endothelial cells and dose-dependently might protect or damage the blood-brain barrier. PLoS One 2024, 19, e0290526.

10.Rong, H.; Li, X.; Yu, C.; Wang, W.; Li, L.; Xu, T.; Ding, Y.; Su, Y.; Wang, X. Targeting the Nrf2-dependent mechanism of β-Ecdysterone in attenuating the motor dysfunction in the MPTP/Pro-induced Parkinson's disease mice model. Folia Neuropathol. 2024, 62, 83–95.

11.Zádor, E. Molecular Targets of 20-Hydroxyecdysone in Mammals, Mechanism of Action: Is It a Calorie Restriction Mimetic and Anti-Aging Compound? Cells 2025, 14, 431.

12.Peng, S.; Wang, L.; Ouyang, J.; Liu, R. Paeoniflorin Combined with Neural Stem Cell Transplantation for

Parkinson's Disease: Dual Mechanism of Cell Therapy and Inflammation Regulation. Drug Des. Devel. Ther. 2025, 19, 7745–7761.

13.Feng, Z.; Jin, C.; Zhang, Y.; Xue, H.; Ai, Y.; Wang, J.; Zheng, M.; Shi, D. Tandem Mass Tags Quantitative Proteomics Reveal the Mechanism by Which Paeoniflorin Regulates the PI3K/AKT and BDNF/CREB Signaling Pathways to Inhibit Parkinson's Disease. Int. J. Mol. Sci. 2025, 26, 6498.

14.Wu, C.; Li, B.; Zhang, Y.; Chen, T.; Chen, C.; Jiang, W.; Wang, Q.; Chen, T. Intranasal delivery of paeoniflorin nanocrystals for brain targeting. Asian J. Pharm. Sci. 2020, 15, 326–335.

15.Hong, D.G.; Lee, S.; Kim, J.; Yang, S.; Lee, M.; Ahn, J.; Lee, H.; Chang, S.C.; Ha, N.C.; Lee, J. Anti-inflammatory and neuroprotective effects of morin in an MPTP-induced PD model. Int. J. Mol. Sci. 2022, 23, 10578.

16.Li, H.Y.; Liu, D.S.; Li, L.B.; Zhang, Y.B.; Dong, H.Y.; Rong, H.; Zhang, J.Y.; Wang, J.P.; Jin, M.; Luo, N.; Zhang, X.J. Total Glucosides of White Paeony Capsule ameliorates Parkinson's disease-like behavior in MPTP-induced mice model by regulating LRRK2/alpha-synuclein signaling. J. Ethnopharmacol. 2024, 319, 117319.

17.Yan, P.; Li, X.; He, Y.; Zhang, Y.; Wang, Y.; Liu, J.; Ren, S.; Wu, D.; Zhao, Y.; Ding, L.; Jia, W.; Lyu, Y.; Xiao, D.; Lin, S.; Lin, Y. The synergistic protective effects of paeoniflorin and β-ecdysterone against cardiac hypertrophy through suppressing oxidative stress and ferroptosis. Cell Signal. 2025, 125, 111509.

18.Liu, H.; Yu, C.; Xu, T.; Zhang, X.; Dong, M. Synergistic protective effect of paeoniflorin and β-ecdysterone against rotenone-induced neurotoxicity in PC12 cells. Apoptosis 2016, 21, 1354–1365.

19.Rong, H.; Sun, X.X.; Li, X.M.; Xu, T.J.; Li, X.; Guo, K.D. Protective effect and mechanism of paeoniflorin on dopaminergic neurons in the substantia nigra of MPTP-induced Parkinson’s disease mice. Zhongguo Xiandai Yixue Zazhi 2022, 24, 18–22.

20.Huang, H.C.; Nguyen, T.; Pickett, C.B. Phosphorylation of Nrf2 at Ser-40 by protein kinase C regulates antioxidant response element-mediated transcription. J. Biol. Chem. 2002, 277, 42769–42774.

21.Costilla, M.; Macri Delbono, R.; Klecha, A.; Cremaschi, G.A.; Barreiro Arcos, M.L. Oxidative Stress Produced by Hyperthyroidism Status Induces the Antioxidant Enzyme Transcription through the Activation of the Nrf-2 Factor in Lymphoid Tissues of Balb/c Mice. Oxid. Med. Cell. Longev. 2019, 2019, 7471890.

22.Liu, Y.; Lin, L.; Zheng, H.; Huang, H.; Qian, Z.J. Microalgae Octapeptide IIAVEAGC Alleviates Oxidative Stress and Neurotoxicity in 6-OHDA-Induced SH-SY5Y Cells by Regulating the Nrf2/HO-1andJak2/Stat3 Pathways. Chem. Biodivers. 2024, 21, e202301509.

23.Xie, S.; Cao, W.; Guo, J.; Zhao, M.; Wang, L.; Liang, F.; Wang, Z. Regulation of HSP90AA1/NRF2 by BDNF Contributes to the Attenuation of Rotenone-Induced Oxidative Stress in Parkinson's Disease Models. Mol. Neurobiol. 2026, 63, 604.

24.Xi, Y.; Tao, K.; Wen, X.; Feng, D.; Mai, Z.; Ding, H.; Mao, H.; Wang, M.; Yang, Q.; Xiang, J.; Zhang, J.; Wu, S.

SIRT3-Mediated Deacetylation of DRP1K711 Prevents Mitochondrial Dysfunction in Parkinson's Disease. Adv. Sci. 2025, 12, e2411235.

25.Wang, Y.; Xu, H.; Chen, S.; Chen, J.; Zheng, Q.; Ma, Y.; Zhao, X.; Shi, Y.; Xiao, L. Oxytocin Protects Nigrostriatal Dopamine Signal via Activating GABAergic Circuit in the MPTP-Induced Parkinson's Disease Model. Adv. Sci. 2024, 11, e2310244.

26.Sheng, Y.C.; Huang, J.N.; Wu, W.L.; Wan, X.R.; Wang, J.; Qin, Z.H.; Wang, Y. TIGAR plays neuroprotective roles in MPP+/MPTP-induced Parkinson's disease by alleviating ferroptosis. Eur. J. Pharmacol. 2025, 995, 177430.

27.Sun, X.; Shen, J.; Shu, Y.; Wang, T.; He, L.; Shen, R.; Zhou, Y.; Cheng, J.; Lin, S.; Ding, J. Deficient AMPK-SENP1-Sirt3 signaling impairs mitochondrial complex I function in Parkinson's disease model. Transl. Neurodegener. 2025, 14, 34.

28.Wang, Q.; Wang, M.; Choi, I.; Sarrafha, L.; Liang, M.; Ho, L.; Farrell, K.; Beaumont, K.G.; Sebra, R.; De Sanctis, C.; Crary, J.F.; Ahfeldt, T.; Blanchard, J.; Neavin, D.; Powell, J.; Davis, D.A.; Sun, X.; Zhang, B.; Yue, Z. Molecular profiling of human substantia nigra identifies diverse neuron types associated with vulnerability in Parkinson's disease. Sci. Adv. 2024, 10, eadi8287.

29.Wang, Y.; Tong, Q.; Ma, S.R.; Zhao, Z.X.; Pan, L.B.; Cong, L.; Han, P.; Peng, R.; Yu, H.; Lin, Y.; Gao, T.L.; Shou, J.W.; Li, X.Y.; Zhang, X.F.; Zhang, Z.W.; Fu, J.; Wen, B.Y.; Yu, J.B.; Cao, X.; Jiang, J.D. Oral berberine improves brain dopa/dopamine levels to ameliorate Parkinson's disease by regulating gut microbiota. Signal Transduct. Target Ther. 2021, 6, 77.

30.Gopinath, A.; Ramirez-Zamora, A.; Franks, S.; Riaz, T.; Smith, A.; Dizon, G.; Hornstein, L.; Follett, J.; Swartz, C.; Bravo, J.; Kugelmann, E.L.; Farrer, M.; Okun, M.S.; Khoshbouei, H. Immunophenotyping Tracks Motor Progression in Parkinson's Disease Associated with a TH Mutation. J. Park. Dis. 2024, 14, 883–888.

31.Liu, J.; Jia, G.; Zhou, Y.; Zhang, J.; Wang, Y.; Cai, Y. UBC9 mediates mitophagy to attenuate oxidative stress by regulating SUMOylation of PINK1 in the Parkinson's disease progression. Cell Biol. Toxicol. 2025, 42, 9.

32.Liu, T.; Kong, X.; Qiao, J.; Wei, J. Decoding Parkinson's Disease: The interplay of cell death pathways, oxidative stress, and therapeutic innovations. Redox Biol. 2025, 85, 103787.

33.Gu, H.Y.; Liu, N.; Lin, F.X.; Yin, J. Nrf2 signaling pathway: focus on oxidative stress in osteoporosis. Osteoporos Int. 2025, 36, 1837–1854.

34.Wu, D.; Sun, Q.; Wei, W.; Bai, Y.; Zhai, L.; Jia, L. Nrf2-mediated protective effect of alpha-lipoic acid on synaptic oxidative damage and inhibition of PKC/ERK/CREB pathway in bisphenol A-exposed HT-22 cells. Food Chem. Toxicol. 2023, 181, 114112.

35.El-Far, Y.M.; Khodir, A.E.; Emarah, Z.A.; Ebrahim, M.A.; Al-Gayyar, M.M.H. Chemopreventive and hepatoprotective effects of genistein via inhibition of oxidative stress and the versican/PDGF/PKC signaling pathway in

experimentally induced hepatocellular carcinoma in rats by thioacetamide. Redox Rep. 2022, 27, 9–20.

36.Hassan, A.; Kungyal, T.; Zhou, S.; Blati, M.; Finnson, K.; Bertos, N.; Golabi, N.; Sadeghi, N.; Loganathan, S.; Philip, A. IL-6-mediated tumorigenicity and antioxidant state in squamous cell carcinoma cells are driven by CD109 via stabilization of IL-6 receptor-alpha and activation of STAT3/NRF2 pathway. Exp. Hematol. Oncol. 2025, 14, 64.

37.Sun, L.; Wilke Saliba, S.; Apweiler, M.; Akmermer, K.; Herlan, C.; Grathwol, C.; deOliveira,A.C.P.;Normann,C.;Jung,N.;Bräse,S.;Fiebich,B.L.Anti-Neuroinflammatory Effects of a Macrocyclic Peptide-Peptoid Hybrid in Lipopolysaccharide-Stimulated BV2 Microglial Cells. Int. J. Mol. Sci. 2024, 25, 4462.

38.Yang, X.; Yv, Q.; Ye, F.; Chen, S.; He, Z.; Li, W.; Dong, F. Echinacoside Protects Dopaminergic Neurons Through Regulating IL-6/JAK2/STAT3 Pathway in Parkinson's Disease Model. Front. Pharmacol. 2022, 13, 848813.

39.Shen, Y.; Li, X.; Wei, D.; Guo, H.; Yang, X.; Zhu, H. Synergistic effects of diammonium glycyrrhizinate and vitamin D3 against EMT in pulmonary fibrosis through modulating the crosstalk of STAT3/HSP90AA1 and HIF-1α pathway. J. Ethnopharmacol. 2026, 359, 120649.

40.Bowden, J.L.; Carr, J.E.; Gabriel, K.A.; Streicher, J.M. Inhibition of heat shock protein 90 in the mouse spinal cord enhances opioid antinociception through upregulation of PKCβ in CGRP neurons. Pain 2026, 167, 2073–2086.

Statements and Declarations

Ethics approval and consent to participate

All animal experimental procedures were reviewed and approved by the Animal Ethics Committee of Qiqihar Medical University (Approval No. QMU-AECC-2025-232). Animal handling and experiments were performed in strict accordance with national guidelines and institutional regulations for the welfare and use of laboratory animals.

Consent for publication

Not applicable.

Data availability

The raw data supporting the findings of this study are not publicly available but are available from the corresponding author upon reasonable request.

Competing interests

The authors have no relevant financial or non-financial interests to disclose.

Funding

This work was supported by the Natural Science Foundation of Heilongjiang Province (Grant No. PL2025H309), the Fundamental Research Funds for the Provincial Undergraduate Universities of Heilongjiang Province (Grant No. 2023-KYYWF-0857), and the Key Discipline Construction Project of Qiqihar Medical University (QYZDXK-011, Pathology).

Author contributions

Xinmin Shi (first author) and Jiaxiang Zhao (co-first author): manuscript drafting and data analysis. Hua Rong: manuscript revision. Xiaoming Li, Xu Li, Haiying Dong, Jingyan Zhang, Tianjiao Xu, Chunlei Yu and Hui Li: study conception and design. All authors read and approved the final manuscript.

Acknowledgements

We thank Hua Rong for providing the experimental platform, Jiaxiang Zhao for guidance on immunohistochemistry and animal experiments, and Xiaoming Li, Xu Li, Haiying Dong, Jingyan Zhang, Tianjiao Xu, Chunlei Yu and Hui Li for their assistance in animal experiments.